Synthesis, characterisation and biological evaluation of monometallic Re(i) and heterobimetallic Re(i)/Fe(ii) complexes with a 1,2,3-triazolyl pyridine chelating moiety

Silvio Jakopec, Lisa Gourdon-Grünewaldt, Ivona Čipor, Andrijana Meščić Macan, Berislav Perić, Ivo Piantanida, Kevin Cariou, Gilles Gasser, Srećko I Kirin, Silvana Raić-Malić

Synthesis, Characterisation and Biological Evaluation of Monometallic Re(I) and Heterobimetallic Re(I)/Fe(II) Complexes with a 1,2,3-Triazolyl Pyridine Chelating Moiety

Silvio Jakopec,[a,†] Lisa Gourdon-Grünewaldt,[b,†] Ivona Čipor,[c,†] Andrijana Meščić Macan,[a] Berislav Perić,[d] Ivo Piantanida,[c] Kevin Cariou,[b] Gilles Gasser,[b,*] Srećko I. Kirin[d,*] and Silvana Raić-Malić[a,*]

Bioorganometallic complexes have attracted considerable interest and have shown promise for potential application in the treatment and diagnosis of cancer, as well as bioimaging agents, some acting as theranostic agents. The series of novel ferrocene, benzimidazo[1,2-*a*]quinoline and fluorescein derivatives with bidentate pyridyl-1,2,3-triazole and 2,2'-dipyridylamine and their tricarbonylrhenium(I) complexes were prepared and fully characterised by NMR, single-crystal X-ray diffraction, UV-Vis and fluorescence spectroscopy in biorelevant conditions. The fluorescein and benzimidazo[1,2-*a*]quinoline ligands and their complexes with Re(I) showed interactions with ds-DNA/RNA and HSA, characterised by thermal denaturation measurements, fluorimetric and circular dichroism titrations. The binding constants revealed that addition of Re(I) increases affinity of fluorescein but decreases affinity of benzimidazo[1,2-*a*]quinoline. The complexation of Re(I) had opposite effect on fluorescein and benzimidazo[1,2-*a*]quinoline ligands fluorimetric sensitivity upon biomacromolecules binding, Re(I) fluorescein complex emission being strongly quenched by DNA/RNA or HSA, while emission of Re(I) benzimidazo[1,2-*a*]quinolone complex was enhanced, particularly for HSA, making it promising fluorescence probe. Some mono- and heterobimetallic complexes showed considerable antiproliferative activity on colon cancer cells (CT26 and HT29), with ferrocene dipyridylamine complexes exhibiting the best inhibitory activity, comparable to cisplatin. The correlation of the cytotoxicity data with the linker type between the ferrocene and the 1,2,3-triazole ring suggests that direct binding of the metallocene to the 1,2,3-triazole is favourable for antitumor activity. The Re(I) benzimidazo[1,2-*a*]quinolone complex showed moderate antiproliferative activity, in contrast to the Re(I) fluorescein complex, which exhibited weak activity on CT26 cells and no activity on HT29 cells. The accumulation of the Re(I) benzimidazo[1,2-*a*]quinolone complex in the lysosomes of CT26 cells indicates the site of its bioactivity, thus making this complex a potential theranostic agent.

Introduction

Platinum coordination compounds cisplatin (**I**), carboplatin (**II**) and oxalilplatin (**III**) (Figure 1), that are used worldwide in cancer chemotherapy,[1,2] are known to be non-specific and target random DNA regions leading to extensive side effects and development of secondary malignancies.[3] Chemoresistance of cancer cells to cisplatin-based chemotherapy presents another serious healthcare issue and limits its clinical use.[4] Following the success of platinum-based drugs and with the aim of developing drugs with fewer side-effects and less prone to induce drug resistance, an important number of metal-containing compounds were investigated.[5–10]

A breakthrough in organometallic chemistry occurred with the discovery of ferrocene and the antiproliferative properties of ferrocenium salts.[11] Ferrocene is particularly attractive because of its stability in aqueous media, favourable electrochemical properties, nontoxicity, and ease of substitution at the cyclopentadienyl rings.[12–14] Ferrocene has been integrated into the structure of established anticancer and antimalarial pharmaceuticals with the purpose of increasing their bioactivity (Figure 1).[15,16] Thus, ferrocifens, ferrocene analogues of tamoxifen (**IV**), showed anticancer activity against breast cancer cells superior to the parent drug.[17,18] A ferrocene-chloroquine conjugate, ferroquine is an antimalarial drug candidate in phase II clinical trials[19,20] that has also shown antitumor activity.[21] In addition, a series of ferrocene-containing heterometallics have been prepared as potential anticancer chemotherapeutics.[22] For example, the organometallic rhodium-ferrocene complexes **V** showed cytotoxicity in prostate cancer cells similar to cisplatin but with a different pathway of cell death.[22] Conjugate of ferrocene and cyretrenyl connected by the imine linker (**VI**) showed antitumor activity superior to cisplatin against hormone-dependant (MCF-7) and hormone-independent (MDA-MB-231) breast cancer cells, along with cisplatin-resistant colon (HCT-116) cancer cell lines, but was also cytotoxic to normal human skin fibroblast (BJ) cells.[23] Tricarbonylrhenium(I) complexes have found potential application as catalysts in various organic reactions,[24,25] photosensitizers in photodynamic cancer therapy,[26,27] probes in fluorescent cell imaging,[28–30] and antiproliferative agents.[6–8,31–34] For example, rhenium(I) bipyridinyl complexes **VII** and **VIII** showed strong inhibition of colorectal cancer and appeared to be safer and more effective than sunitinib, doxorubicin or cisplatin. In the zebrafish xenograft model of colorectal carcinoma, the complexes inhibited tumor growth, vascularization and tumor cells metastasis without inducing cardio-, hepato-, and myelotoxicity.[35] A series of water-coordinated Re(I) complexes proved effective against cervical carcinoma (HeLa), several wild-type and cisplatin-resistant cell lines, with the 2,9-dimethyl-1,10-phenanthroline complex **IX** being the most active, and were also less toxic to human fibroblast cells compared to cisplatin.[36]

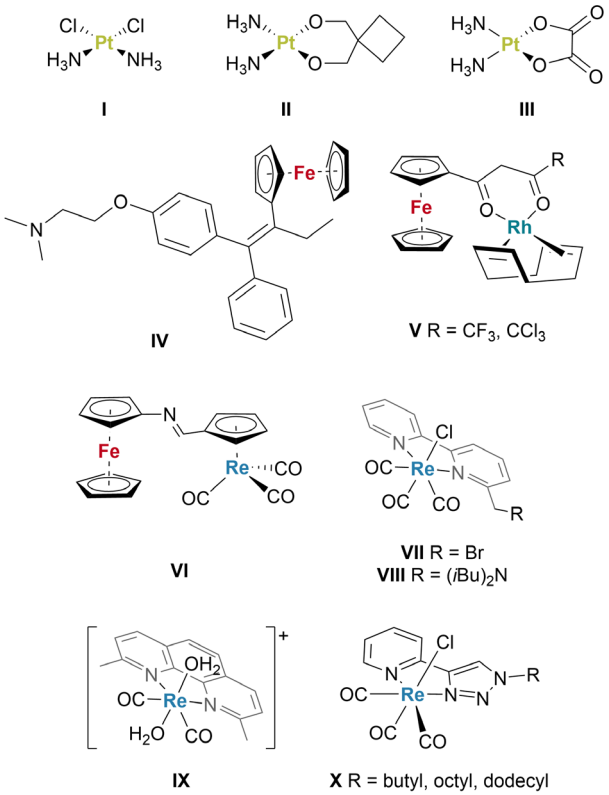

Figure 1. Examples of antitumor organometallic complexes.

There is an increasing interest in the development of bi-, tri- and polydentate ligand architectures incorporating 1,2,3-triazolyl based donor ligands[37,38] that can coordinate metals at the N-3, N-2 and C-5 donor sites.[39,40] For example, several luminescent tricarbonylrhenium(I) complexes (**X**), with the lipophilic aliphatic side chains at the ligand proved effective against breast cancer (MDA-MB-231) cells, with the positive correlation of cytotoxicity with the permeability.[41]

Exploitation of luminescent organometallic complexes for cell imaging is a rapidly developing research field, which has received attention in the last few years.[30,42] Most fluorescent probes are highly conjugated fused heterocyclic derivatives.[43] The octahedral Re(I) complexes with bidentate nitrogen ligands, showed luminescence and good physicochemical properties, pointing out the potential use as fluorescent dyes for cell imaging.[44–47]

Detailed studies of interactions of novel organometallic complexes with biomolecules are useful for providing information on potential targets of these compounds[48] and these interactions, mainly with DNA, can be correlated with antiproliferative activities.[49] Three main ways in which compounds can reversibly bind to polynucleotides are intercalation, minor/major groove binding or through electrostatic interactions.[50] Transition metal complexes have been extensively studied in this area of research.[51–53] For example, coumarin derived rhenium (I) complexes were shown to be minor groove binders,[49] while 1,10-phenanthroline-5,6-dione Re(I) complexes interacted with the major groove of DNA, showing that both ligands and geometrical orientation of organometallic complexes can direct the binding mode and in turn alter the biological activity.[54]

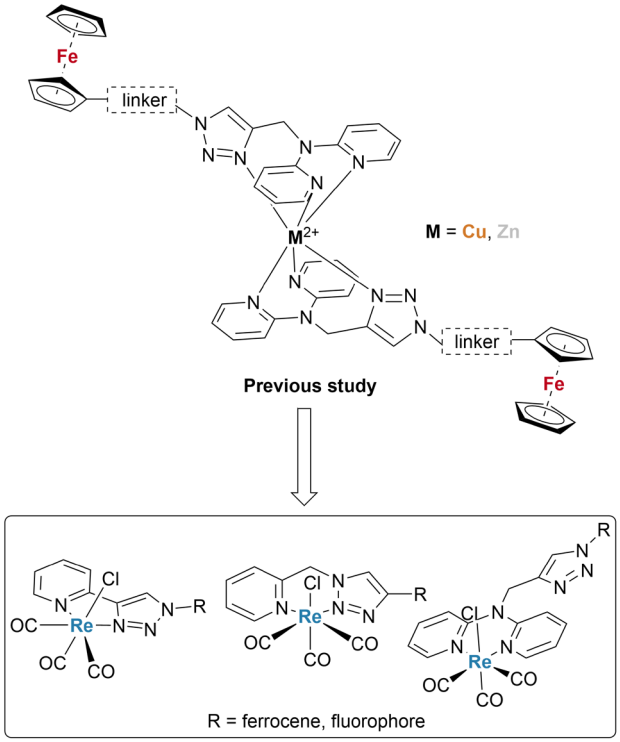

Figure 2. Design of 1,2,3-triazolyl pyridine tricarbonylrhenium(I) complexes containing ferrocene, and fluorescein and ring-fused biheterocyclic[55] pharmacophore.

In our previous study,[56] we described Cu(II) complexes of a series of ferrocene and aromatic amine conjugates linked by 1,2,3-triazole (Figure 2) that showed increased antiproliferative activity against cervical (HeLa), ovarian (MES-OV), non-small cell lung (A549) and breast (MDA-MB-231) cancer cell lines compared to the activity of the parent ligand molecules. Fluorescein, that is commonly employed in cellular biology as a tracer, after photoactivation showed to significantly decrease the viability of human hepatoblastoma HepG2 cells,[57] while benzimidazo[1,2-*a*]quinoline derivatives showed pronounced antiproliferative activity, particularly on colon cancer (HCT116) cell lines.[55,58]

Within the context above, we have designed ferrocene-appended tricarbonylrhenium(I) complexes with the pyridyl-1,2,3-triazolyl, dipyridylamine and dipyridylamine-1,2,3-triazolyl chelating moiety (Figure 2), which coordinates the Re(I) metal centre, with the aim to evaluate their antiproliferative activity. In order to assess interactions of the synthesised compounds with biomolecules and cell imaging, structural analogues of heterobimetallic Re(I) complexes in which the ferrocene moiety was replaced by fluorescein and a benzimidazo[1,2-*a*]quinoline fluorophore and their monometallic fluorescent Re(I) complexes were synthesized (Figure 2).

Results and discussion

Synthesis

The target ferrocene-appended 1,2,3-triazolyl pyridine ligands (**2a**–**2c**, **3** and **4a**–**4b**) and their rhenium(I) complexes (**2a$_{Re}$**–**2c$_{Re}$**, **3$_{Re}$** and **4a$_{R}$**–**4b$_{Re}$**) were synthesised following procedures depicted in Scheme 1. The 1,2,3-triazole ligands with the 2-pyridyl substituent attached at C-4 position (**2a**,[59] **2b**,[60] **2c**) were synthesised by copper-catalysed azide-alkyne cycloaddition reaction (CuAAC) of 2-ethynylpyridine with the corresponding ferrocene azide (**1a**–**1c**).[61] Copper(II) acetate monohydrate was reduced in methanol to provide copper(I) catalyst for the CuAAC reaction. 2-Picolyl-substituted 1,2,3-triazole ligand **3**[60] was prepared from 2-picolylazide and ethynylferrocene using the same method. The reaction was completed within 0.5 h. This rapid azide-alkyne cycloaddition can be explained by the ability of 2-picolylazide to form a complex with Cu(II) ions which leads to an accelerated azide-alkyne cycloaddition.[62] The dipyridylamine ligands **4a**–**4b** (dpa) were prepared following a previously reported procedure,[56] which included alkylation of 2,2'-dipyridylamine with propargyl bromide and sodium hydride, followed by CuAAC reaction with corresponding ferrocenyl azide **1a**–**1b**.

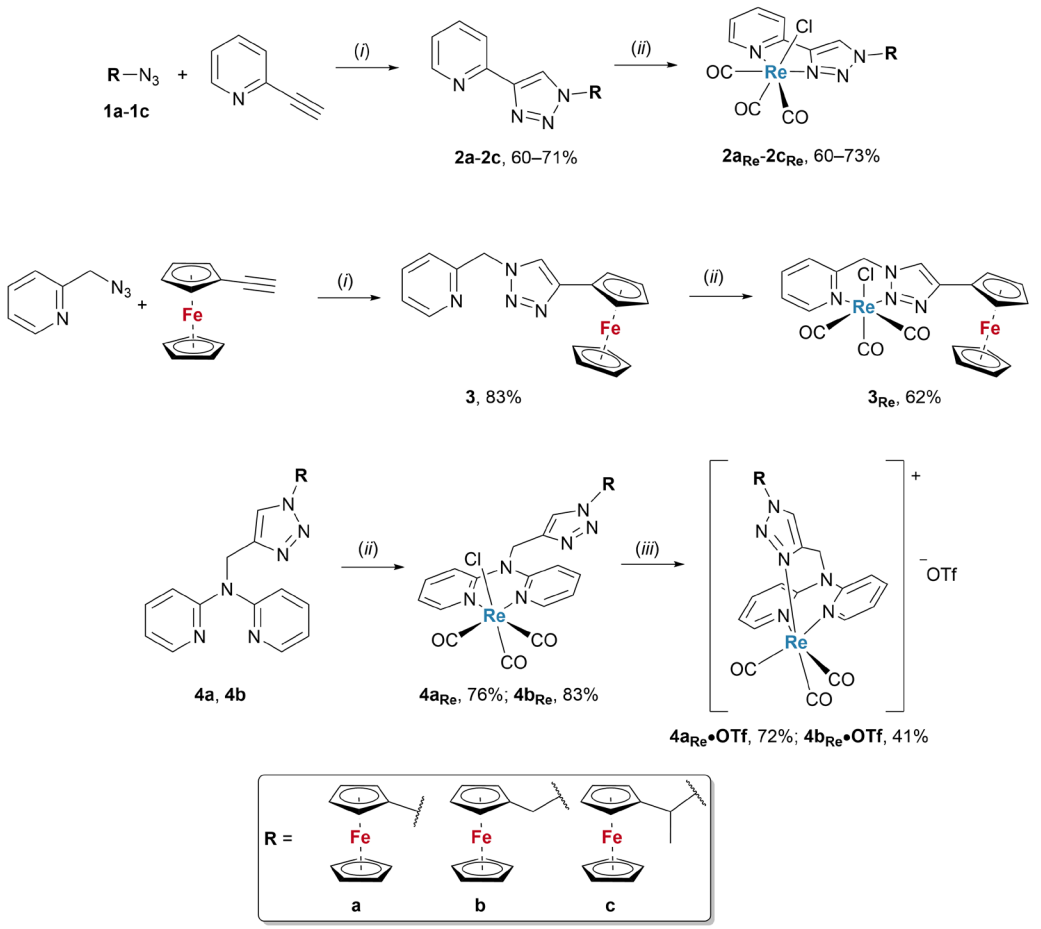

Scheme 1. Synthesis of heterobimetallic Re(I) complexes. Reagents and reaction conditions: (*i*) $Cu(OAc)_2 \cdot H_2O$, MeOH, r. t., 20–24 h; (*ii*) $Re(CO)_5Cl$, $CHCl_3$, 60 °C, 24 h; (*iii*) AgOTf, ACN, 14 h

Rhenium(I) complexes were prepared by the complexation reaction of ligands with pentacarbonylrhenium(I) chloride as the metal precursor. Complexation reactions and the purification of metal complexes was performed in the dark because of the photosensitive nature of Re(I) complexes (see the General remarks section for more details). Bidentate coordination of metal ion in complexes **2a$_{Re}$**–**2c$_{Re}$** and **3$_{Re}$** occurs by pyridine and N-3 and N-2 1,2,3-triazole nitrogen atoms, respectively. On the other hand, coordination of Re(I) in **4a$_{Re}$**–**4b$_{Re}$** by 2,2'-dipyridylamine (dpa) group is preferred over coordination of 1,2,3-triazole nitrogen atom. Coordination by dpa prompted us to perform an anion exchange reaction in which the chloride anion is replaced by a triflate. The reaction is accompanied by a change of the coordination mode from bidentate to tridentate, along with the formation of positively charged complex cations **4a$_{Re}$·OTf** and **4b$_{Re}$·OTf**.

Contrary to previous reports on fluorescent Re(I) complexes of related structure,[41,63,64] complexes **2a$_{Re}$**–**2c$_{Re}$**, **3$_{Re}$**, **4a$_{Re}$**–**4b$_{Re}$** and their triflate analogues **4a$_{Re}$·OTf**–**4b$_{Re}$·OTf** did not exhibit luminescent properties. This can be rationalised by the well-known fluorescence quenching effect of ferrocene.[65] Thereafter, the ferrocene moiety was replaced with fluorescein and a ring-fused biheterocyclic fluorophore. The propargyl intermediate **5** was prepared by a previously published two-step synthesis[66] which included the esterification of fluorescein in methanol under acidic conditions and subsequent alkylation of the product with propargyl bromide and potassium carbonate as a base (Schemes 2, top and S1).

Click reaction of the alkyne **6** with 2-picolylazide yielded the corresponding 1,2,3-triazole ligand **6a**. By complexation of **6a** with $Re(CO)_5Cl$ in chloroform, rhenium(I) complex **6a$_{Re}$** was obtained. Regarding the synthesis of complex **9$_{Re}$**, benzimidazo[1,2-*a*]quinoline core was prepared by a multi-step synthesis reported earlier.[55] The azide intermediate **8** was prepared from 5-chlorobenzimidazo[1,2-*a*]quinoline-6-carbonitrile (**7**) by nucleophilic aromatic substitution with sodium azide in acetonitrile (Scheme 2, bottom). The 1,2,3-triazole linker was subsequently formed by the CuAAC reaction of the azide **8** and 2-ethynylpyridine which afforded ligand **9**. Complex **9$_{Re}$** was prepared by complexation reaction of ligand **9** with $Re(CO)_5Cl$ in chloroform.

Solid state characterisation

Single crystals of two ligands, isomers **2b** and **3**, suitable for structure determination by single-crystal X-ray diffraction were obtained by slow evaporation from dichloromethane : methanol solutions (Figure S3). 1,2,3-Triazole derivative **2b** is substituted by 1-ferrocenemethyl group at the C-1 and 2-pyridyl substituent at N-1 of the heterocyclic core. Pyridine atom N_{Py} is in the *trans*-conformation to the 1,2,3-triazole ring. Ligand **3** differs from its isomer **2b** in configuration around the linker ring, where the former has ferrocene substituent attached at the C-4 of 1,2,3-triazole core and N-1 substituent is 2-picolyl group. As opposed to the previous example, occupancy of N_{Py} of the picolyl group in the ligand **3** is 72% for the *cis*-conformation (towards the 1,2,3-triazole), and 28% for the *trans*-conformation. Crystals of $\mathbf{2a_{Re}}$, $\mathbf{3_{Re}}$ and $\mathbf{4a_{Re}}$ were obtained by slow evaporation from dichloromethane : methanol solutions, while $\mathbf{4b_{Re}}$**·OTf** crystallizes from $CDCl_3$ (Figure 3). In $\mathbf{2a_{Re}}$, $\mathbf{3_{Re}}$ and $\mathbf{4a_{Re}}$ the ligands coordinate the metal ion in bidentate fashion, with octahedral geometry and a N_2C_3Cl coordination sphere around Re(I). *Fac*-stereochemistry was observed in the crystal structures of the complexes, owing to the back-bonding influence of the CO ligands.[67] The metal centre is coordinated by N_{Py} and N-3 of the triazole ring in $\mathbf{2a_{Re}}$, and by N_{Py} and N-2 of the triazole in the isomeric complex $\mathbf{3_{Re}}$.

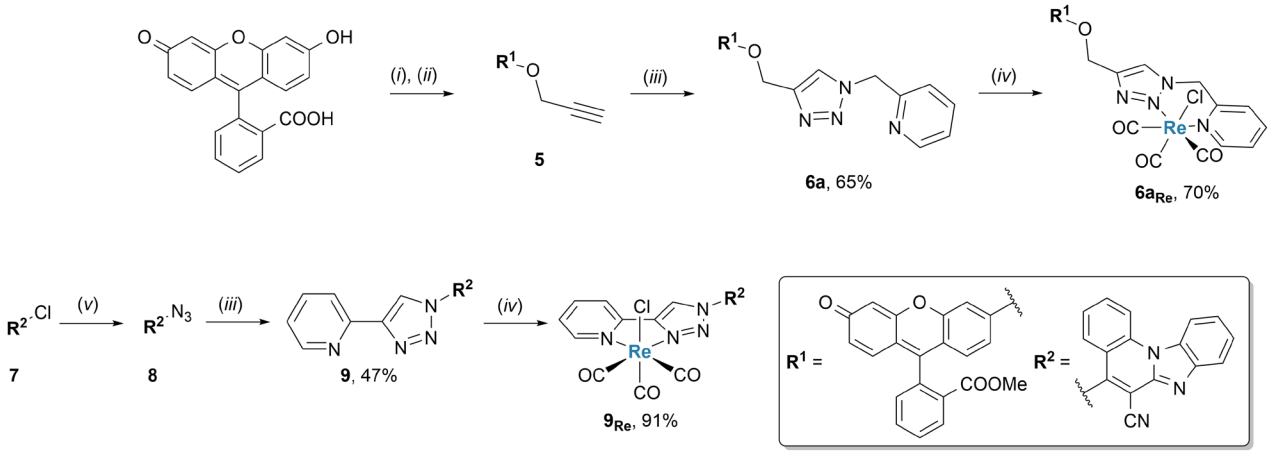

Scheme 2. Synthesis of fluorescent rhenium(I) complexes ($\mathbf{6a_{Re}}$ and $\mathbf{9_{Re}}$). Reagents and conditions: *i)* H_2SO_4, MeOH, 14 h, 85 °C; *ii)* propargyl bromide, K_2CO_3, r. t., 24 h; *iii)* 2-picolylazide for **6a**, 2-ethynylpyiridine for **9**, $Cu(OAc)_2{\cdot}H_2O$, MeOH, r. t., 20–24 h; *iv*) $Re(CO)_5Cl$, $CHCl_3$, 60 °C, 14 h; *v)* NaN_3, MeCN, 4 h, 80 °C

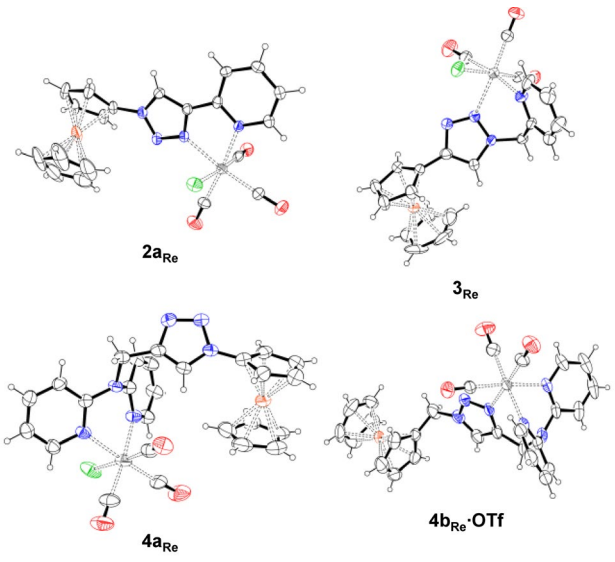

Figure 3. Crystal structures of complexes $\mathbf{2a_{Re}}$, $\mathbf{3_{Re}}$, $\mathbf{4a_{Re}}$ and $\mathbf{4b_{Re}}$**·OTf**. For $\mathbf{3_{Re}}$ only one symmetry independent molecule and only position of Re atom with occupancy > 90% is shown. The full labelling schemes are shown in Figure S4. Colour scheme: brown–Fe; grey–Re; green–Cl, red–O; blue -N and black–C and H (small circles).

In the complex $\mathbf{4a_{Re}}$, Re(I) ion is coordinated by two N_{Py} donors of dpa. Chloride ion is covalently bonded to the metal centre in aforementioned complexes. Exchange of chloride with triflate counterion to obtain $\mathbf{4b_{Re}}$**·OTf**, containing a cationic complex, promotes coordination of Re(I) by N_{Tz} donor. *Fac*-stereochemistry of the complex is retained. Geometry of $\mathbf{4b_{Re}}$**·OTf** is distorted octahedral, with one pyridine coordinated axially and the other coordinated equatorially, similarly to the structure of $\mathbf{4a_{Re}}$.

Contrary to our previously reported structure of [Cu(**4a**)$_2$]OTf$_2$[56] in which Py rings arrange in equatorial positions and the triazole ring is coordinated in apical coordination site, one pyridine and triazole of dpa in **4b$_{Re}$·OTf** are coordinated at an equatorial site, while the second pyridine is bonded axially to the metal centre.

Spectroscopic characterisation

The ^{1}H NMR spectra of ligands **2a**–**2c**, **3**, **4a**–**4b** show characteristic signals for corresponding protons of the ferrocene ring, as well as downfield resonances of H5-triazole and pyridine protons (Figures S28–S46). Chemical shifts of protons of fluorophores in **6a**, **6b** and **9** correspond to previously published spectral data.[55,68]

Compared to the free ligand, the ^{1}H NMR and ^{13}C NMR spectra of rhenium(I) complexes show downfield shifts due to the deshielding effect of a metal ion. Expectedly, for complexes in which the 1,2,3-triazole ring is included in chelation of rhenium(I), the largest shifts were observed for proton of the triazole ring ($\Delta\delta \approx 0.5$ ppm) and the pyridine proton in *ortho* position to the N-donor atom ($\Delta\delta \approx 0.3$ ppm). In addition to the downfield shift of the methylene protons, in the ^{1}H NMR spectrum of **3$_{Re}$** and **6a$_{Re}$** the two α-CH$_2$ protons are no longer equivalent and show two doublets with large geminal coupling (J = 16 Hz). Figure 4 illustrates the trends in chemical shifts upon coordination of **4b** with the Re(I) ion. Both triazole and pyridine protons experience strong deshielding effects, with the *ortho* pyridine shifting for $\Delta\delta$ = 0.6 ppm and triazole proton for $\Delta\delta$ = 0.4 ppm. Interestingly, in the spectrum of the triflate salt (**4b$_{Re}$·OTf**) the values of chemical shifts of H5 and H5' protons (green) are significantly increased. ^{13}C NMR spectra of metal complexes show three signals at 197-189 ppm, corresponding to carbon atoms of the carbonyl group, indicating presence of [Re(CO)$_3$Cl] in the structures of the metal complexes.

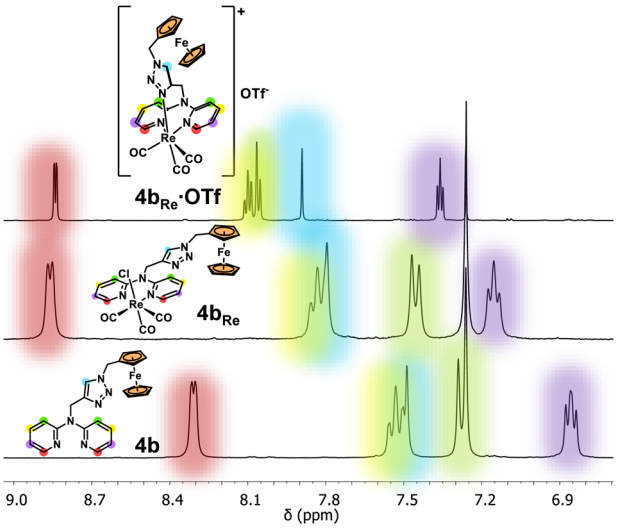

Figure 4. Comparison of proton NMR spectra of ligand **4b** and its complexes ($CDCl_3$)

In the IR spectra of Re(I) complexes (Figures S47–S65), three bands in the region of 2030–1890 cm^{-1} are observed for symmetric and asymmetric stretching of carbonyl groups, which are indicative of the *fac*-stereochemistry of carbonyl groups around the metal centre.[69] UV-Vis spectra of ferrocene ligands and complexes (Figures S66–S70) show an absorption peak at about 450 nm, owning to d-d transitions or by a metal-ligand charge transfer process, characteristic for ferrocene derivatives.[59,70,71] Derivatives **6a**, **6b** and complex **6a$_{Re}$** show absorption maxima at λ_{max} = 431, 454 and 484 nm, while benzimidazo[1,2-*a*]quinoline **9** and its metal complex **9$_{Re}$** show absorption maximum at λ_{max} = 272 and 363 nm in the UV region, along with a shoulder at λ_{sh} = 414 nm in the visible part of the spectrum (Figures S66-S70).

Spectroscopic characterisation and interactions of 6a, 6a$_{Re}$, 9 and 9$_{Re}$ with biomolecules

Fluorescent rhenium(I) complexes **6a$_{Re}$** and **9$_{Re}$** and their ligands **6a** and **9** were chosen due to their structural and emissive properties for detailed study of interactions with ds-DNA or ds-RNA and proteins, namely the model protein human serum albumin (HSA). First, ligands **6a** and **9**, as well as their rhenium(I) complexes **6a$_{Re}$** and **9$_{Re}$** were spectroscopically characterised. Stock solutions of **6a**, **9**, **6a$_{Re}$** and **9$_{Re}$** were prepared in DMSO at $c = 1 \times 10^{-3}$ M and kept at 4 °C, being stable for more months. Working aliquots were prepared prior to any experiment from stock solutions and kept at 25 °C.

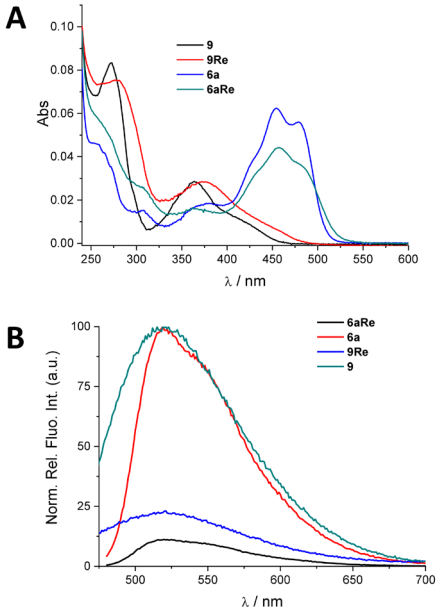

Figure 5. UV/Vis (A, c = 2 × 10^{-6} M) and fluorescence spectra (B, c = 2 × 10^{-6} M) of studied compounds in water, normalised to maximum emission of ligands **6a** and **9**, and spectra of $\mathbf{6a_{Re}}$ and $\mathbf{9_{Re}}$ divided by difference in fluorescence quantum yield from ligand values (Φ_F, Table 1).

Absorbance of aqueous solutions of all compounds and Re(I) complexes was proportional to concentration up to c = 2 × 10^{-5} M (Figure S72-76), yielding molar extinction coefficients (Table 1, ε) and excluding intermolecular interactions or aggregation of compounds. The UV/Vis spectra of complexes $\mathbf{6a_{Re}}$ and $\mathbf{9_{Re}}$ differed from spectra of ligands (Figure 5A), demonstrating change of electronic properties for chromophores upon complexation of Re(I). UV/Vis spectra of complexes were strongly dependent on temperature (Figure S79), suggesting decomposition of complexes at high temperature.

Studied ligands **6a** and **9** and their Re(I) complexes showed emission maximums around 520 nm, regardless of the structure (Figure 5B). However, the fluorescein **6a** and its analogue $\mathbf{6a_{Re}}$ showed higher quantum yield values (Table 1) in respect to **9** and $\mathbf{9_{Re}}$, while the latter showed larger Stokes shifts (Table 1). Fluorescence intensity changes were linear with an increase in concentration (Figure S80) and dependent on temperature (Figure S81), irreversibility of emission upon cooling back to room temperature attributed to the Re(I) complex decomposition at higher temperatures. The quantum yield values of both ligands are higher than that of their complexes and fluorescence decay times became shorter upon Re(I) complexation (Table 1), suggesting that rhenium(I) enables non-radiative decay and thus quenches the fluorescence of these ligands.

Fluorimetric titrations

Taking advantage of the fluorescence of studied compounds and their Re(I) complexes, we performed fluorimetric titrations to investigate the interactions with biomacromolecules. Namely, we have chosen ct-DNA as representative of ds-DNA B-helical structures and poly A–poly U as representative of ds-RNA A-helical structures. Further, we studied interactions with human serum albumin (HSA), as one of the most abundant protein in plasma, acting as a carrier for a variety of small molecules, including hormones, fatty acids but also drugs and toxins.[72]

The addition of ds-polynucleotides to aqueous solutions of compounds resulted in the strong quenching of fluorescence emission (Figure 6). The titration data fitting to Scatchard equation,[73] yielded binding constants (Table 2, log K_s).

Table 1. Electronic absorption and emission data of **6a**, **6a$_{Re}$**, **9** and **9$_{Re}$** in water

Compound	λ_{max}/ nm	λ_{em}/nm	[c]ε/M^{-1}cm^{-1}	[a]Φ_F/%	Stokes shift/nm	[b]τ/ns	χ^2
6a	454 479	520	26962 30046	42.1	41	2.72	1.096
6a$_{Re}$	460	520	18139	15.8	60	0.42 2.67	1.094
9	368 272	518	9038 24044	6.2	150	0.88 4.4 15.75	1.141
9$_{Re}$	376 278	520	13048 29768	1.1	144	0.16 0.99 3.37	0.984

[a]Absolute fluorescence quantum yield was determined by integrating sphere SC-30, Edinburgh Inst., for Argon purged solutions, by λ_{max} of the longest wavelength maximum (λ_{max}), at pH 7.0, sodium cacodylate buffer, I = 0.05 M.
[b]Solutions were purged by argon and excited by pulsing diode at 405 (**9**,**9$_{Re}$**) or 450 (**6a**,**6a$_{Re}$**) nm. The measurements were performed three times and the average values are reported. The associated errors correspond to the maximum absolute deviation, at pH 7.0, sodium cacodylate buffer, I = 0.05 M.
[c]In water.

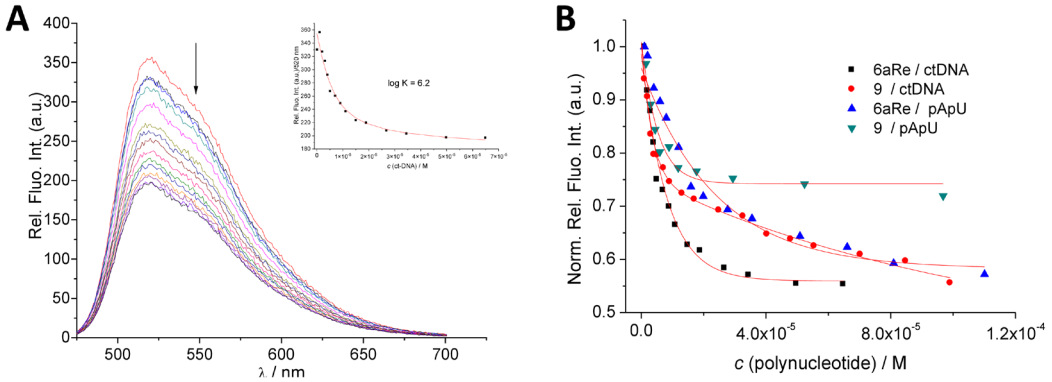

Figure 6. A) changes in fluorescence spectrum of **6a$_{Re}$** (c = 1 × 10^{-6} M, λ_{exc} = 460 nm, λ_{em} = 520 nm) upon titration with ctDNA at pH 7.0, sodium cacodylate buffer, I = 0.05 M; inset–dependence of **6a$_{Re}$** intensity at λ_{max} = 520 nm on c(ct-DNA), at pH 7.0, sodium cacodylate buffer, I = 0.05 M fit to Scatchard equation, B) dependence of **6a$_{Re}$** and **9** intensity at λ_{max} = 520 nm on c(polynucleotide), at pH 7.0, sodium cacodylate buffer, I = 0.05 M

Table 2. Binding constants (log K_s) and emission quenching efficiency (ΔInt[a]) for **6a**, **6a$_{Re}$**, **9** and **9$_{Re}$** with polynucleotides[b] and HSA[c], determined from fluorimetric titrations, done in sodium cacodylate buffer (pH = 7.0, I = 0.05 M).

Compound		[b]ct-DNA	[a]pApU	[c]HSA
6a	log K_s	[d]	[d]	4.2
	ΔInt	-	-	0.2
6a$_{Re}$	log K_s	6.2	5.4	6.1
	ΔInt	0.5	0.6	0.6
9	log K_s	6.1	6.8	5.8
	ΔInt	0.5	0.8	0.2
9$_{Re}$	log K_s	5-6[c]	[d]	4.1
	ΔInt	-	-	4.7

[a]ΔInt = Int/Int$_0$, [b]Processing of titration data by Scatchard equation gave values of ratio n[bound dye]/[polynucleotide] = 0.2 and 0.3. For ease of comparison, all log Ks values were recalculated for fixed n = 0.2. Correlation coefficients were >0.99 for all calculated K_s. [c]The best fit obtained for 1:1 stoichiometry dye:HSA, [d]too small changes for accurate processing.

Intriguingly, the complexation of Re(I) had opposite effect on fluorimetric response of ligands. The emission of fluorescein **6a** only negligibly changed upon addition of ds-DNA or ds-RNA (Figures S82, S83), whereas emission of analogue complex **6a$_{Re}$** was strongly quenched (Figure 8A, Figure S85). Opposite effect was observed for benzimidazo[1,2-*a*]quinoline derivative **9**, whereby

ligand **9** responded to addition of ds-DNA/RNA by strong emission quenching but Re(I) complex **9a$_{Re}$** showed only very weak emission increase (Figures S87, S88, S90, S91). Calculated binding constants (Table 2) were in line with emission intensity change, being higher for **9a$_{Re}$** in comparison to ligand **9**, whereas it was not possible to determine interaction of ligand **6** with DNA/RNA. Therefore, complexation of Re(I) can work in both ways, depending on the structure of the ligand.

Interactions with protein HSA even more stressed the importance of Re(I) complexation. For instance, addition of HSA induced strong emission quenching of ligand **9** (Figure S89), while its complex **9$_{Re}$** showed increase in emission upon binding to HSA (Figure S92). Adversely, addition of HSA to aqueous solutions of **6a** and **6a$_{Re}$** resulted in quenching of their emission (Figure S84, S86). The obtained binding constants (Table 2) revealed that addition of Re(I) increases the affinity of **6a** but decreases the affinity of **9**.

CD experiments

To further analyse the binding modes, circular dichroism measurements were performed. Circular dichroism is a sensitive spectroscopic method which can show subtle changes in the secondary structures of DNA/RNA, as well as changes occurring upon the formation of polynucleotide/small molecule complexes.[74] Small achiral molecules can acquire an induced circular dichroism spectrum (ICD) upon binding to chiral polynucleotides, which in turn can suggest the dominant mode of interaction.[75]
The compounds **9** and **9$_{Re}$** only influence the spectra of DNA or RNA in the range of 260 to 300 nm (Figures S94, S95), suggesting a decrease of polynucleotide helical chirality, more pronounced for RNA than DNA. Addition of the fluorescein ligand **6a** also induced a similar small decrease in the CD spectrum of DNA/RNA (260 to 300 nm) accompanied by a very weak negative ICD band around 450–460 nm, in agreement with the maximum of fluorescein absorbance (Figure S93). This could be indicative of intercalative binding.[75] Addition of the complex **6a$_{Re}$** induced comparable change in the 260–300 nm range, thus confirming binding to ds-DNA/RNA (Figure S93), although the absence of ICD bands points out that complexation of Re(I) changed the geometry of the ligand and that **6a$_{Re}$** has different orientation in the binding site, with respect to the polynucleotide chiral axis.

Thermal melting experiments

Thermal dissociation of ds-DNA/RNA is a well-defined process occurring at a specific temperature (T_m value) and as such can be implemented for the characterisation of polynucleotide/small molecule complexes and polynucleotide related processes.[76] The addition of small molecules to ds-polynucleotides can result in the stabilisation (increase) or destabilisation (reduction) of T_m value. The difference in T_m value of free polynucleotides and T_m values of polynucleotides with non-covalently bound small molecules (ΔT_m value) can be used in characterisation of the binding mode. For example, moderate to strong stabilisation (ΔT_m > 5 °C) supports minor-groove binding or intercalative interactions,[77] while weak to moderate stabilisation (ΔT_m = 0–5 °C) indicates a binding process driven by weak H-bonding, hydrophobic effects or electrostatic interactions or any combination of these interactions.

Table 3. ΔT_m values for different ratios [a]*r* of the dyes added to polynucleotide obtained through thermal melting experiments

Compound	[a]*r*	ΔT_m ct-DNA	ΔT_m pApU
6a	0.1	+1± 0.5 °C	-
	0.2	-0.6± 0.5 °C	-
6a$_{Re}$	0.1	-	-
	0.2	+2.6± 0.5 °C	-1.5 ± 0.5 °C
9	0.1	+3.1± 0.5 °C	+1.6± 0.5 °C
	0.2	+1.4± 0.5 °C	-
9$_{Re}$	0.1	+1.3± 0.5 °C	+1.2 ± 0.5 °C
	0.2	+2.3± 0.5 °C	+2± 0.5 °C

[a]*r* = [compound]/[polynucleotide]

Thermal denaturation measurements were performed in ratios *r* = 0.1 or *r* = 0.2 for all the studied compounds with both polynucleotides. The results show only minor stabilisation of ds-polynucleotides for ligand **9** and its complex **9$_{Re}$**, while **6a** and **6a$_{Re}$** showed no effect on stabilisation of ds-RNA (Table 3, Figures S96–S100). For ds-DNA, **6a** showed negligible effect, while complex **6a$_{Re}$** increased the stability of ds-DNA by 2.6 °C at a ratio of 0.2 (Table 3, Figure S96). These results agree well with fluorimetric titrations (Table 2), thus pointing out that ligand **6** does not interact with ds-DNA or ds-RNA, whereas its Re(I) complex **6a$_{Re}$** showed biorelevant interactions. Consequently, ICD signals obtained in circular dichroism studies observed for **6a** do not stem from intercalation into DNA, but more likely from non-specific hydrophobic aggregation along the polynucleotide. On the other hand, all results obtained for derivatives **9** and **9$_{Re}$** support interaction with ds-DNA and ds-RNA, the absence of specific ICD signals suggesting heterogeneous binding within DNA/RNA grooves.

Cytotoxicity evaluations on 2D monolayer cells

Cytotoxicity activity of Re(I) complexes (**2a$_{Re}$**–**2c$_{Re}$**, **3$_{Re}$**, **4a$_{Re}$**–**4b$_{Re}$**, **4a$_{Re}$·OTf**–**4b$_{Re}$·OTf**, **6a$_{Re}$** and **9$_{Re}$**) was determined by the resazurin assay on murine (CT26) and human (HT29) colorectal carcinoma cells. Cytotoxicity of the most active complexes **4a$_{Re}$** and **4b$_{Re}$**, as

well as the fluorescent complex **9$_{Re}$** was also investigated on human retinal pigment epithelial-1 (RPE-1) cells to assess if some degree of selectivity towards cancer cells existed (Figures S101–124). Cisplatin (CDDP) was used as a reference compound. The results are presented in Table 4.

Table 4. The cytotoxic activity of complexes **2a$_{Re}$–2c$_{Re}$**, **3$_{Re}$**, **4a$_{Re}$–4b$_{Re}$**, **4a$_{Re}$·OTf**, **4b$_{Re}$·OTf**, **6a$_{Re}$** and **9$_{Re}$** towards CT26, HT29 and RPE-1 cell lines

Complex	IC$_{50}$ ± SD /μM		
	CT26	HT29	RPE-1
2a$_{Re}$	11.7 ± 0.3	34.0 ± 1.0	–
2b$_{Re}$	19.9 ± 2.5	49.9 ± 1.9	–
2c$_{Re}$	13.5 ± 2.3	54.8 ± 0.2	–
3$_{Re}$	22.7 ± 1.6	53.8 ± 0.9	–
4a$_{Re}$	5.1 ± 0.9	44.4 ± 1.2	10.6 ± 0.1
4b$_{Re}$	5.6 ± 1.4	35.4 ± 1.9	16.0 ± 0.6
4a$_{Re}$·OTf	12.6 ± 1.2	40.4 ± 0.7	–
4b$_{Re}$·OTf	13.1 ± 0.5	36.5 ± 1.6	–
6a$_{Re}$	40.3 ± 1.4	>100	–
9$_{Re}$	13.8 ± 0.9	43.4 ± 0.9	8.0 ± 0.1
CDDP[b]	6.8 ± 0.1	10.2 ± 0.6	46.5 ± 3.1

[a]50% inhibitory concentration or compound concentration required to inhibit tumor cell proliferation by 50%. Data represent the mean IC$_{50}$ (μM) value of three independent experiments each evaluated on 3 replicates ± SD (IC$_{50}$ μM ± SD). [b]CDDP–cisplatin

The difference between the cytotoxic activities of the tested complexes was dependant on both bidentate or tridentate coordination and type of the coordinating group (Figure 7). The most active compounds were dipyridylamine complexes **4a$_{Re}$** and **4b$_{Re}$**, with IC$_{50}$ values on CT26 cell line in the range of cisplatin. This antiproliferative effect was not specific to cancer cells: **4a$_{Re}$** and **4b$_{Re}$** showed similar IC$_{50}$ values on RPE-1 healthy cell line. Complexes **2a$_{Re}$–2c$_{Re}$** with bidentate ligands showed moderate cytotoxic activity. Similar activity is exhibited by positively charged complexes **4a$_{Re}$·OTf** and **4b$_{Re}$·OTf**.

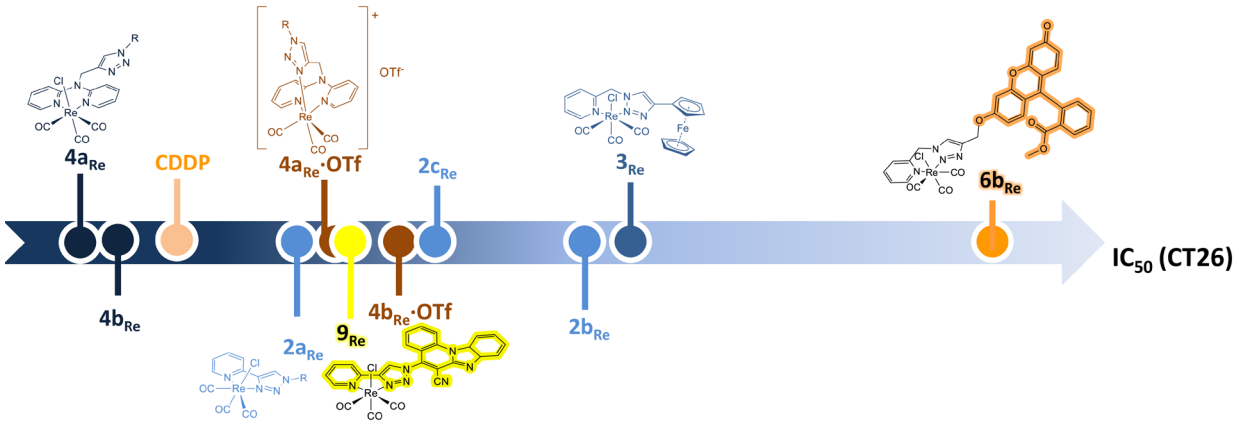

Figure 7. Decreasing from left to right: the antiproliferative activity of Re(I) complexes towards CT26 cell line.

Changing the coordination mode from bidentate in **4a$_{Re}$** and **4b$_{Re}$** to tridentate in **4aRe·OTf** and **4bRe·OTf** decreased the antiproliferative effect of the **4aRe·OTf** and **4bRe·OTf** complexes on CT26 cells, which may be related to their conformationally restricted structures due to the coordination of both the dipyridylamine and 1,2,3-triazole units. Antiproliferative evaluation of ligands **4a** and **4b** for the most active complexes (**4a$_{Re}$**, **4b$_{Re}$**, **4a$_{Re}$·OTf** and **4b$_{Re}$·OTf**) on cervical carcinoma (HeLa), ovarian cancer (MES-OV), non-small cell lung cancer (A549) and breast carcinoma (MDA-MB-231) cell[56] showed that ligands **4a** and **4b** exhibited low inhibitory effect on evaluated carcinoma cell lines, thus confirming that coordination of the ferrocene-appended 1,2,3-triazolyl pyridine ligands with rhenium(I) improved antiproliferative activity compared to the parent ligands.

The type of linker between ferrocene and the 1,2,3-triazole moiety also affected the antiproliferative activity, showing that metallocene directly attached to 1,2,3-triazole is favourable for the activity. The comparable cytostatic effects of **2b$_{Re}$** and **3$_{Re}$** complexes suggest that the mode of coordination with N-3 and N-2 donor atoms (regular vs. inverse)[78] of the 1,2,3-triazole ring has a negligible influence on the cytostatic activity. Chosen representatives of studied Re-complexes (**4a$_{Re}$**, **4b$_{Re}$**, **6a$_{Re}$** and **9$_{Re}$**) were

additionally evaluated for their stability in cell culture medium, showing no significant changes in their UV/Vis spectra over 24 h (Figures S125–128).

Generally, all tested complexes showed more than three-fold lower activity on human HT29 cells compared to that on CT26 cells, with IC_{50} values in the range 34.0-54.8 μM towards HT29 cells. For example, complexes **2a$_{Re}$** and **4b$_{Re}$** exerted moderate activity on HT29 cells with IC_{50} values of 34.0 and 35.4 μM, respectively.

Among the fluorescent complexes, **9$_{Re}$** showed notable inhibitory activity against CT26 cell line, about twice the IC_{50} of cisplatin. However, the cytotoxicity on RPE-1 healthy cells was found to be in the same concentration range, showing no selectivity towards cancer cells. Fluorescein derivative **6a$_{Re}$** exhibited low cytotoxic activity on CT26 cells and no activity on HT29 cells.

Confocal microscopy

The localization of the most cytotoxic, fluorescent complex **9$_{Re}$** was established by confocal microscopy (Figure 8, Figures S129–S132). Confocal imaging allowed us to show that the complex is localized in lysosomes. This localization of the complex can be explained by the neutral, lipophilic and slightly basic structure of the ligand 9. It can be assumed that once in the lysosome, the complex is protonated (lysosomes being acidic), which would then prevent the compound from crossing the membrane and leave the organelle.[79,80]

Conclusions

Pyridine (**2a**–**2c**, **3**) and 2,2'-dipyridylamine (**4a**–**4b**) ligands were prepared by cycloaddition of 2-ethynylpyridine and *N*-propargyl-2,2'-dipyridylamine with ferrocene azides catalyzed by copper(I) and subsequently used as ligands for the synthesis of heterobimetallic complexes with Re(I). Fluorescein (**6a**) and benzimidazo[1,2-*a*]quinoline (**9**) ligands were additionally prepared and used in the synthesis of monometallic tricarbonylrhenium(I) complexes. Crystal structures of isomers **2b** and **3** and complexes **2a$_{Re}$**, **3$_{Re}$** and **4a$_{Re}$** with bidentate coordination and complex **4b$_{Re}$·OTf** with tridentate coordination were determined. Crystal structures confirmed the ML stoichiometry and *fac*-stereochemistry; the latter can be attributed to the influence of π-back donation of CO ligands. Dipyridylamine complexes **4a$_{Re}$** and **4b$_{Re}$** showed the most prominent antiproliferative activity against CT26 cell line, similar to that of reference cisplatin. On the contrary, pyridine triazole complexes **2a$_{Re}$**–**2c$_{Re}$** showed moderate inhibitory activity. The type of the linker between the ferrocene and the 1,2,3-triazole ring had an influence on cytotoxicity, indicating that the direct binding of metallocene to 1,2,3-triazole is favourable for the antitumor activity. The benzimidazo[1,2-*a*]quinoline complex **9$_{Re}$** showed moderate antiproliferative activity, while the fluorescein (**6a$_{Re}$**) exhibited weak activity on CT26 cells and no activity on HT29 cells.

Detailed analysis of interactions of **9$_{Re}$** and **6a$_{Re}$** with biomacromolecules revealed that both Re(I) complexes interact with ds-DNA, ds-RNA and HSA with biorelevant affinity. Of particular interest was the opposite fluorescence response of ligand **9** (quenching) and complex **9$_{Re}$** (emission increase) to HSA, which could be used in detection of Re(I) in plasma.

The **9$_{Re}$** colocalisation in CT26 cells with LysoTracker™ points out to the possible site of its antiproliferative activity, suggesting that it does not target nuclear DNA as potential mechanism of action. Further design of benzimidazo[1,2-*a*]quinoline analogues by means of ring-fused biheterocyclic Re(I) complexes may lead to the development of novel theranostic lysosome-targeting anticancer agents.

To the best of our knowledge, complexes **4a$_{Re}$** and **4b$_{Re}$** are the first examples of heterobimetallic Re(I) complexes containing ferrocene that strongly affected the viability of colorectal carcinoma cells, while monometallic complex **9$_{Re}$** is the first metal-based compound with benzimidazo[1,2-*a*]quinoline pharmacophore.

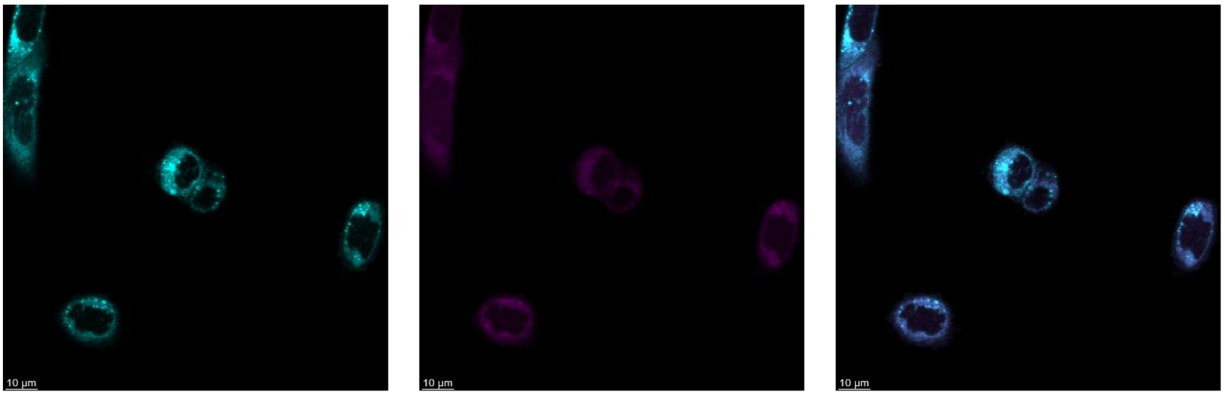

Figure 8. Confocal imaging in a CT26 cell line after 3 h of incubation with 7 µM of $\mathbf{9_{Re}}$ complex (magenta). Cells were labeled with LysoTracker™ Deep Red (cyan). All scale bars: 10 µm. On the left: Lysotracker fluorescence. In the middle: $\mathbf{9_{Re}}$ fluorescence (7 µM). On the right: overlay.

Experimental section

General remarks

Reactions were carried out in ordinary glassware, and chemicals were purchased from commercial suppliers and used without further purification. Precoated Merck (Darmstadt, Germany) silica gel 60F-254 plates were used for thin-layer chromatography and the spots were detected under UV light (254 and 366 nm). Column chromatography was done using Fluka (Buchs, Switzerland) silica gel (0.063-0.2 mm). Glass columns were slurry-packed under gravity. ^{1}H and ^{13}C NMR spectra were acquired on a Bruker 300 and 600 MHz NMR spectrometer (Bruker Biospin, Rheinstetten, Germany). Chemical shifts were referenced to the signal of DMSO-d_6 at δ = 2.50 ppm (^{1}H NMR) and δ = 39.50 ppm (^{13}C NMR), $CDCl_3$ at δ = 7.26 ppm (^{1}H NMR) and δ = 77.16 ppm (^{13}C NMR) and CD_3CN at δ = 1.94 ppm (^{1}H NMR) and δ = 118.26 ppm (^{13}C NMR). Individual resonances were assigned on the basis of their chemical shifts, signal intensities, multiplicity of resonances and H–H coupling constants. Elemental composition analyses were performed on Perkin Elmer 2400 Series II CHNS analyser. Compositions of all novel compounds were within 0.4% of the calculated values. Melting points (uncorrected) were determined with Kofler hot-stage microscopy (Reichert, Wien, Austria). IR spectra were recorded using KBr pellets with a Bruker Alpha FT-IR spectrometer, in the 4000−350 cm^{-1} region or PerkinElmer Spectrum ONE FT-IR with Universal UATR Sampling Accessory, in the 4000−650 cm^{-1} region. UV/Vis absorption spectra of ligands and their rhenium(I) complexes were recorded at the concentration of 1 x 10^{-3} mol dm^{-3} and 2 x 10^{-5} mol dm^{-3} in acetonitrile (HPLC grade) using a Varian Cary 50 spectrophotometer operated in double-beam mode at 25 °C. The covered wavelength range was 200–500 nm. Quartz cells of 1 cm path length were used and absorbancies were sampled at 0.1 nm intervals.

Synthesis of precursors and derivatives **1a**-**1c**[61], 2-picolyl azide[81], **2a**[59], $\mathbf{2a_{Re}}$[82], **2b**[60], **3**[60], **4a**[56], **4b**[56], **5**[68] and **8**[55] was described previously in the literature. Precursors were prepared according to the previously described procedures, while ligands and metal complexes were prepared according to modified procedures.

The synthesis and isolation of rhenium(I) complexes were performed in the dark due to the photosensitivity of the compounds. For this purpose, the used glassware was wrapped in aluminium foil while performing complexation reactions, isolating the complex by column chromatography and removing the solvent by vacuum evaporation. Complexes were stored in the dark.

General procedure for the synthesis of ligands

The alkyne (1 equiv.) and copper(II) acetate monohydrate (0.05 equiv.) were added to the solution of the corresponding azide (1-1.1 equiv.) in methanol (5 ml). The reaction mixture was stirred at room temperature for 20-24 h. After the reaction was completed the solvent was evaporated under reduced pressure. The product of the reaction was isolated by column chromatography.

1-Ferrocenyl-4-(2-pyridyl)-1,2,3-triazole (2a).[59] Compound **2a** was synthesised according to the general procedure using 1-azidoferrocene (**1a**, 200 mg, 0.88 mmol, 1 equiv.), 2-ethynylpyridine (90 µl, 0.88 mmol) and $Cu(OAc)_2{\cdot}H_2O$ (8 mg, 0.04 mmol, 0.05 equiv.) in methanol (5 ml). Mobile phase for column chromatography was dichloromethane : methanol = 50 : 1. Yield: **2a** (0.55 mmol, 63%), yellow crystals (m. p. > 200 °C). ^{1}H NMR (300 MHz, DMSO) δ 9.08 (s, 1H, H5-triaz.), 8.65 (d, *J* = 4.6 Hz, 1H, Ar-H), 8.09 (d, *J* = 7.9 Hz, 1H, Ar-H), 7.93 (t, *J* = 8.5 Hz, 1H, Ar-H), 7.46–7.32 (m, 1H, Ar-H), 5.24–5.07 (m, 2H, Fc-H), 4.44–4.32 (m, 2H, Fc-H), 4.22 (s, 5H, Fc-H). ^{13}C NMR (151 MHz, DMSO) δ 149.55, 137.26, 133.30, 132.14, 123.17, 122.16, 119.63, 93.31, 69.93, 66.67, 61.60. IR (ATR)/cm^{-1}: 3080, 1735, 1605 (sp^2 C=N stretch), 1516 (sp^2 C=C Ar stretch), 1467 (sp^2 C=C Ar stretch), 1426 (sp^2 C=C Ar stretch), 1395, 1239, 1150, 1102, 1029, 999, 872, 811, 778, 743, 737, 712.

1-Ferrocenemethyl-4-(2-pyridyl)-1,2,3-triazole (2b).[60] Compound **2b** was synthesised according to the general procedure using 1-azidomethylferrocene (**1b**, 200 mg, 0.58 mmol, 1 equiv.), 2-ethynylpyridine (59 µl, 0.58 mmol) and $Cu(OAc)_2 \cdot H_2O$ (5 mg, 0.029 mmol, 0.05 equiv.) in methanol (5 ml). Mobile phase for column chromatography was dichloromethane : methanol = 50 : 1. Yield: **2b** (0.35 mmol, 60%), yellow crystals (m. p. = 179–180 °C). Needle-like orange crystals of **2b** suitable for crystal structure determination were obtained by slow evaporation from a dichloromethane : methanol solution. ^{1}H NMR (300 MHz, CD_3CN) δ 8.57 (d, *J* = 4.5 Hz, 1H, Ar-H), 8.21 (s, 1H, H5-triaz.), 8.07 (d, *J* = 7.9 Hz, 1H, Ar-H), 7.83 (td, *J* = 7.8, 1.8 Hz, 1H, Ar-H), 7.33–7.25 (m, 1H, Ar-H), 5.38 (s, 2H, CH_2), 4.46–4.32 (m, 2H, Fc-H), 4.23 (s, 6H, Fc-H), 4.06 (s, 1H, Fc-H). ^{13}C NMR (75 MHz, DMSO) δ 149.94, 149.54, 147.17, 137.14, 122.90, 122.71, 119.32, 82.30, 68.71, 68.63, 68.40, 49.13. IR (ATR)/cm^{-1}: 3089 (sp^2 C-H stretch), 2968 (sp^3 C-H stretch), 1746 (sp^2 C=N stretch), 1592 (sp^2 C=C Ar stretch), 1470 (sp^2 C=C stretch), 1467 (sp^2 C=C Ar stretch), 1454 (sp^2 C=C Ar stretch), 1417, 1366, 1334, 1220, 1193, 1193, 1146, 1076, 1072, 1041, 998, 925, 845, 819, 774, 746, 721.

1-(1-Ferroceneethyl)-4-(2-pyridyl)-1,2,3-triazole (2c). Compound **2c** was synthesised according to the general procedure using 1-azidomethylferrocene (**1c**, 200 mg, 0.56 mmol, 1 equiv.), 2-ethynylpyridine (57 µl, 0.56 mmol) and $Cu(OAc)_2 \cdot H_2O$ (5 mg, 0.03 mmol, 0.05 equiv.) in methanol (5 ml). Mobile phase for column chromatography was dichloromethane : methanol = 50 : 1. Yield: **2c** (0.40 mmol, 71%), yellow crystals (m. p. = 162–164 °C). ^{1}H NMR (300 MHz, DMSO) δ 8.57 (d, *J* = 4.9 Hz, 2H, Ar-H and H5-triaz.), 8.01 (d, *J* = 7.9 Hz, 1H, Ar-H), 7.87 (td, *J* = 7.8, 1.6 Hz, 1H, Ar-H), 7.38–7.26 (m, 1H, Ar-H), 5.76 (q, *J* = 7.0 Hz, 1H, CH), 4.44 (s, 1H, Fc-H), 4.28 (s, 1H, Fc-H), 4.18 (s, 7H, Fc-H), 1.91 (d, *J* = 7.0 Hz, 3H, CH_3). ^{13}C NMR (75 MHz, DMSO) δ 149.99, 149.49, 146.96, 137.14, 122.88, 121.23, 119.30, 88.41, 68.73, 68.20, 67.78, 67.40, 66.23, 55.90, 20.65. IR (ATR)/cm^{-1}: 3093 (sp^2 C-H stretch), 2988 (sp^3 C-H stretch), 2937 (sp^3 C-H stretch), 1734 (sp^2 C=N stretch), 1605 (sp^2 C=C Ar stretch), 1568, 1547, 1471, 1418, 1382, 1353, 1301, 1247, 1220, 1155, 1102, 1037, 1025, 993, 914, 846, 817, 779, 746, 723, 708.

4-Ferrocenyl-1-(2-picolyl)-1,2,3-triazole (3).[60] Compound **3** was synthesised according to the general procedure using 2-picolylazide (160 mg, 1.20 mmol, 1 equiv.), ethynylferrocene (252 mg, 1.20 mmol, 1 equiv.) and $Cu(OAc)_2 \cdot H_2O$ (11 mg, 0.06 mmol, 0.05 equiv.) in methanol (5 ml). Mobile phase for column chromatography was dichloromethane : methanol = 50 : 1. Yield: **3** (1.00 mmol, 83%), orange crystals (m. p. = 160–162 °C). Needle-like orange crystals of **3** suitable for crystal structure determination were obtained by slow evaporation from a dichloromethane : methanol solution. ^{1}H NMR (300 MHz, CD_3CN) δ 8.56 (d, *J* = 4.3 Hz, 1H, Ar-H), 7.86 (s, 1H, H5-triaz.), 7.77 (td, *J* = 7.7, 1.7 Hz, 1H, Ar-H), 7.31 (dd, *J* = 7.2, 5.0 Hz, 1H, Ar-H), 7.24 (d, *J* = 7.8 Hz, 1H, Ar-H), 5.64 (s, 2H, CH2), 4.73–4.66 (m, 2H, Fc-H), 4.31–4.25 (m, 2H, Fc-H), 4.03 (s, 5H, Fc-H). ^{13}C NMR (151 MHz, CD_3CN) δ 156.23, 150.59, 147.25, 138.23, 124.17, 122.99, 121.69, 76.93, 70.31, 69.36, 67.47, 55.94. IR (ATR)/cm^{-1}: 3109 (sp^2 C-H stretch), 3073 (sp^2 C-H stretch), 2918 (sp^3 C-H stretch), 2847 (sp^3 C-H stretch), 1592 (sp^2 C=N stretch), 1437 (sp^2 C=C Ar stretch), 1345, 1227, 1152, 1107, 1050, 1000, 878, 808, 752, 712.

***N,N*-di-2-pyridyl-((1-ferrocenyl-1,2,3-triazol-4-yl)methyl)amine (4a).**[56] Compound **4a** was synthesised according to the general procedure using 1-azidoferrocene (**1a**, 85 mg, 0.38 mmol, 1 equiv.), *N*-propargyl-di(2-pyridyl)amine (85 mg, 0.41 mmol, 1.1 equiv.) and $Cu(OAc)_2 \cdot H_2O$ (4 mg, 0.02 mmol, 0.05 equiv.) in methanol (7.5 ml). Mobile phase for column chromatography was cyclohexane:ethyl acetate = 1:1. Yield: **4a** (0.23 mmol, 60 %), yellow powder (m. p. = 154–155 °C). ^{1}H NMR (400 MHz, DMSO) δ 8.37–8.29 (m, 2H, Ar-H), 8.20 (s, 1H, H5-triaz.), 7.72–7.62 (m, 2H, Ar-H), 7.30 (d, *J* = 8.4 Hz, 2H, Ar-H), 7.03–6.93 (m, 2H, Ar-H), 5.46 (s, 2H, CH_2), 4.97 (pt, *J* = 1.9 Hz, 2H, Fc-H), 4.28 (pt, *J* = 1.9 Hz, 2H, Fc-H), 4.05 (s, 5H, Fc-H). ^{13}C NMR (101 MHz, DMSO) δ 156.14, 147.83, 145.30, 137.59, 122.89, 117.41, 114.65, 93.36, 69.72, 66.41, 61.70, 42.93. IR (ATR)/cm^{-1}: 2966 (sp^3 C-H stretch), 2931 (sp^3 C-H stretch), 2875 (sp^3 C-H stretch), 1703 (sp^2 C=N stretch), 1564 (sp^2 C=C Ar stretch), 1467 (sp^2 C=C Ar stretch), 1435 (sp^2 C=C Ar stretch), 1373, 1206, 1157, 1058, 993, 880, 773, 754, 664.

***N,N*-di-2-pyridyl-((1-ferrocenemethyl-1,2,3-triazol-4-yl)methyl)amine (4b).**[56] Compound **4b** was synthesised according to the general procedure using 1-azidomethylferrocene (**1b**, 180 mg, 0.75 mmol, 1.1 equiv.), *N*-propargyl-di(2-pyridyl)amine (122 mg, 0.67 mmol, 1 equiv.) and $Cu(OAc)_2 \cdot H_2O$ (7 mg, 0.04 mmol, 0.05 equiv.) in methanol (6 ml). Mobile phase for column chromatography was cyclohexane:ethyl acetate = 1:1. Yield: **4b** (0.29 mmol, 43 %), yellow powder (m. p. = 90–92 °C). ^{1}H NMR (400 MHz, DMSO) δ 8.41–8.18 (m, 2H, Ar-H), 7.84 (s, 1H, H5-triaz.), 7.72–7.57 (m, 2H, Ar-H), 7.26 (d, *J* = 8.4 Hz, 2H, Ar-H), 7.03–6.88 (m, 2H, Ar-H), 5.38 (s, 2H, CH_2), 5.20 (s, 2H, CH_2), 4.21 (pt, *J* = 1.9 Hz, 2H, Fc-H), 4.12 (pt, *J* = 1.9 Hz, 2H, Fc-H), 4.07 (s, 5H, Fc-H). ^{13}C NMR (101 MHz, DMSO) δ 156.63, 148.31, 145.29, 138.06, 123.40, 117.86, 115.00, 83.34, 69.02, 68.84, 68.59, 49.08, 43.66. IR (ATR)/cm^{-1}: 3158, 3052 (sp^2 C-H stretch), 2965 (sp^3 C-H stretch), 2918 (sp^3 C-H stretch), 2856 (sp^3 C-H stretch), 1704 (sp^2 C=N stretch), 1659 (sp^2 C=N stretch), 1563 (sp^2 C=C Ar stretch), 1471 (sp^2 C=C Ar stretch), 1430 (sp^2 C=C Ar stretch), 1381, 1327, 1203, 1149, 1106, 1048, 979, 873, 750.

Methyl 2-(6-((1-(2-picolyl)-1,2,3-triazol-4-yl)methoxy)-3-oxoxanthen-9-yl)benzoate (6a). Compound **6a** was synthesised according to the general procedure using 2-picolylazide (39 mg, 0.29 mmol, 1.1 equiv.), propargyl derivative **5** (100 mg, 0.26 mmol, 1 equiv.) and $Cu(OAc)_2 \cdot H_2O$ (2 mg, 0.01 mmol, 0.05 equiv.) in methanol (7 ml). Mobile phase for column chromatography was dichloromethane : methanol = 30 : 1. Yield: **6a** (0.17 mmol, 65%), red crystals (m. p. = 149–150 °C). ^{1}H NMR (300 MHz, DMSO) δ 8.54 (d, *J* = 4.1 Hz, 1H, H5-triaz.), 8.38 (s, 1H, Ar-H), 8.27–8.17 (m, 1H, Ar-H), 7.94–7.69 (m, 3H, Ar-H), 7.57–7.46 (m, 1H, Ar-H), 7.41 (d, *J* = 2.3 Hz, 1H, Ar-H), 7.39–7.26 (m, 2H, Ar-H), 6.96 (dd, *J* = 8.9, 2.3 Hz, 1H, Ar-H), 6.89–6.74 (m, 2H, Ar-H), 6.40 (dd, *J* = 9.7, 1.9 Hz, 1H, Ar-H), 6.26 (d, *J* = 1.9 Hz, 1H, Ar-H), 5.75 (s, 2H, CH_2), 5.35 (s, 2H, CH_2), 3.59 (s, 3H, OCH_3). IR (KBr)/cm^{-1}: 3055 (sp^2 C-H stretch), 2951 (sp^3 C-H stretch), 2924 (sp^3 C-H stretch), 2850 (sp^3 C-H stretch), 1726 (ester C=O stretch), 1642 (sp^2 C=N stretch),

1595 (sp^2 C=C Ar stretch), 1514 (sp^2 C=C Ar stretch), 1481 (sp^2 C=C Ar stretch), 1456, 1416, 1383, 1276 (C-O stretch), 1255 (C-O stretch), 1211, 1127, 1108, 1082, 1002, 854, 756.

5-(2-Pyridynyl)-1,2,3-triazol-1-yl)benzimidazo[1,2-a]quinoline-6-carbonitrile (9). Compound **9** was synthesised according to the general procedure using the azide **8** (127 mg, 0.44 mmol, 1 equiv.), 2-ethynylpyridine (50 µl, 0.49 mmol, 1.1 equiv.) and $Cu(OAc)_2 \cdot H_2O$ (4 mg, 0.02 mmol, 0.05 equiv.) in methanol (6 ml). Mobile phase for column chromatography was dichloromethane : methanol = 100 : 1. The isolated product was triturated with cold solvents (*n*-hexane, ethanol and methanol). Yield: **9** (0.21 mmol, 47 %), yellow powder (m. p. > 250 °C). ^{1}H NMR (600 MHz, DMSO) δ 9.42 (s, 1H, H5-triaz.), 9.06 (d, *J* = 8.6 Hz, 1H, Ar-H), 8.89 (dd, *J* = 6.6, 2.4 Hz, 1H, Ar-H), 8.76–8.67 (m, 1H, Ar-H), 8.26 (d, *J* = 7.9 Hz, 1H, Ar-H), 8.19–8.10 (m, 2H, Ar-H), 8.04 (td, *J* = 7.8, 1.8 Hz, 1H, Ar-H), 7.75–7.65 (m, 3H, Ar-H), 7.54 (dd, *J* = 8.2, 1.2 Hz, 1H, Ar-H), 7.51-7.46 (m, 1H, Ar-H). ^{13}C NMR (151 MHz, DMSO) δ 149.95, 148.82, 148.06, 144.26, 143.35, 141.66, 137.58, 135.85, 134.92, 130.58, 126.68, 126.50, 126.08, 125.82, 124.67, 123.81, 120.71, 120.13, 118.26, 116.63, 115.26, 112.24, 100.84. IR (KBr)/cm^{-1}: 3113, 2923 (sp^2 C-H stretch), 2851, 2377, 2345, 2319 (C≡N), 2240, 1641 (sp^2 C=N stretch), 1632 (sp^2 C=C Ar stretch), 1611, 1449, 1420, 1384, 1286, 1255, 1023, 798, 749.

General procedure for the synthesis of metal complexes

To the solution of the ligand (1 equiv.) in chloroform was added $Re(CO)_5Cl$ (1 equiv.) and the reaction mixture was stirred in dark at the reflux temperature for 14 h. After completion of the reaction the solvent was evaporated under reduced pressure. The product was isolated by column chromatography with a dichloromethane : methanol mixture as a mobile phase.

Complex 2a$_{Re}$. Ligand **2a** (100 mg, 0.30 mmol, 1 equiv.), $Re(CO)_5Cl$ (109 mg, 0.30 mmol, 1 equiv.) and chloroform (20 ml) were used for the synthesis. Mobile phase for column chromatography was dichloromethane : methanol = 50 : 1. Yield: **2a$_{Re}$** (0.22 mmol, 73 %), yellow crystals (m. p. > 200 °C). Needle-like yellow crystals of **2a$_{Re}$** suitable for crystal structure determination were obtained by slow evaporation from a dichloromethane : methanol solution. ^{1}H NMR (300 MHz, CD_3CN) δ 8.99 (d, *J* = 5.4 Hz, 1H, Ar-H), 8.94 (s, 1H, H5-triaz.), 8.19 (td, *J* = 7.8, 1.4 Hz, 1H, Ar-H), 8.09 (d, *J* = 7.9 Hz, 1H, Ar-H), 7.55 (ddd, *J* = 7.2, 5.6, 1.3 Hz, 1H, Ar-H), 5.10–5.02 (m, 2H, Fc-H), 4.49–4.43 (m, 2H, Fc-H), 4.33 (s, Fc-H). ^{13}C NMR (151 MHz, DMSO) δ 197.44 (Re-CO), 196.53 (Re-CO), 189.47 (Re-CO), 153.00, 148.61, 148.42, 140.58, 126.53, 125.38, 122.75, 99.43, 92.36, 70.42, 67.68, 67.63, 62.94, 62.88. IR (ATR)/cm^{-1}: 2031 (M-C≡O sym. stretch), 1911 (M-C≡O asym. stretch), 1893 (M-C≡O asym. stretch), 1614 (sp^2 C=N stretch), 1583 (sp^2 C=C Ar stretch), 1515 (sp^2 C=C Ar stretch), 1458, 1414, 1267, 1151, 1106, 1089, 1046, 1004, 876, 819, 780, 729. Calc. for $C_{20}H_{14}ClFeN_4O_3Re$: C, 37.78; H, 2.22; N, 8.81, exp. C, 37.56; H, 2.11; N, 8.60.

Complex 2b$_{Re}$. Ligand **2b** (100 mg, 0.29 mmol, 1 equiv.), $Re(CO)_5Cl$ (105 mg, 0.29 mmol, 1 equiv.) and chloroform (20 ml) were used for the synthesis. Mobile phase for column chromatography was dichloromethane : methanol = 50 : 1. Yield: **2b$_{Re}$** (0.20 mmol, 70 %), yellow crystals (m. p. = 199–201 °C). ^{1}H NMR (300 MHz, CD_3CN) δ 8.94 (d, *J* = 5.4 Hz, 1H, Ar-H), 8.50 (s, 1H, H5-triaz.), 8.11 (td, *J* = 7.9, 1.3 Hz, 1H, Ar-H), 8.00 (d, *J* = 7.9 Hz, 1H, Ar-H), 7.50 (ddd, *J* = 7.2, 5.6, 1.2 Hz, 1H, Ar-H), 5.45 (s, 2H, CH_2), 4.42 (d, *J* = 1.7 Hz, 2H, Fc-H), 4.34–4.28 (m, 2H, Fc-H), 4.25 (s, 5H, Fc-H). ^{13}C NMR (151 MHz, DMSO) δ 197.61 (Re-CO), 196.75 (Re-CO), 189.53 (Re-CO), 152.96, 148.67, 148.12, 140.57, 126.41, 125.35, 122.70, 80.58, 68.91, 68.83, 68.81, 68.75, 51.07. IR (ATR)/cm^{-1}: 3083 (sp^2 C-H stretch), 2973 (sp^3 C-H stretch), 2019 (M-C≡O sym. stretch), 1919 (M-C≡O asym. stretch), 1885 (M-C≡O asym. stretch), 1736 (sp^2 C=N stretch), 1614 (sp^2 C=C Ar stretch), 1448 (sp^2 C=C Ar stretch), 1375, 1262, 1220, 1106, 1044, 997, 831, 809, 777, 735. Calc. for $C_{21}H_{16}ClFeN_4O_3Re$: C, 38.81; H, 2.48; N, 8.62, exp. C, 38.85; H, 2.36; N, 8.82.

Complex 2c$_{Re}$. Ligand **2c** (100 mg, 0.28 mmol, 1 equiv.), $Re(CO)_5Cl$ (101 mg, 0.28 mmol, 1 equiv.) and chloroform (20 ml) were used for the synthesis. Mobile phase for column chromatography was dichloromethane : methanol = 50 : 1. Yield: **2c$_{Re}$** (0.14 mmol, 50 %), yellow crystals (m. p. = 163–165 °C). ^{1}H NMR (300 MHz, CD_3CN) δ 8.94 (d, *J* = 5.4 Hz, 1H, Ar-H), 8.52 (d, *J* = 2.8 Hz, 1H, H5-triaz.), 8.11 (td, *J* = 7.8, 1.2 Hz, 1H, Ar-H), 7.99 (d, *J* = 7.9 Hz, 1H, Ar-H), 7.54–7.45 (m, 1H, Ar-H), 5.89 (p, *J* = 6.9 Hz, 1H, CH), 4.43–4.37 (m, 1H, Fc-H), 4.32–4.25 (m, 3H, Fc-H), 4.25–4.14 (m, 5H, Fc-H), 2.00 (dd, *J* = 7.0, 1.5 Hz, 3H, CH_3). ^{13}C NMR (151 MHz, DMSO) δ 197.61 (Re-CO), 196.76 (Re-CO), 189.55 (Re-CO), 152.97, 148.76, 148.73, 147.97, 147.95, 140.57, 126.40, 124.20, 124.05, 122.61, 122.58, 87.52, 87.34, 68.95, 68.92, 68.56, 68.47, 68.17, 68.10, 67.02, 66.39, 66.33, 58.29, 58.25, 20.89, 20.81. IR (ATR)/cm^{-1}: 3092 (sp^2 C-H stretch), 2980 (sp^3 C-H stretch), 2016 (M-C≡O sym. stretch), 1911 (M-C≡O asym. stretch), 1872 (M-C≡O asym. stretch), 1740 (sp^2 C=N stretch), 1610 (sp^2 C=C Ar stretch), 1584 (sp^2 C=C Ar stretch), 1458, 1368, 1233, 1120, 1025, 1025, 1003, 828, 771, 744. Calc. for $C_{22}H_{18}ClFeN_4O_3Re$: C, 39.80; H, 2.73; N, 8.44, exp. C, 39.91; H, 2.84; N, 8.31.

Complex 3$_{Re}$. Ligand **3** (100 mg, 0.29 mmol, 1 equiv.), $Re(CO)_5Cl$ (105 mg, 0.29 mmol, 1 equiv.) and chloroform (20 ml) were used for the synthesis. Mobile phase for column chromatography was dichloromethane : methanol = 50 : 1. Yield: **3$_{Re}$** (0.18 mmol, 62 %), yellow crystals (m. p. > 200 °C). Needle-like yellow crystals of **3$_{Re}$** suitable for crystal structure determination were obtained by slow evaporation from a dichloromethane : methanol solution. ^{1}H NMR (300 MHz, CD_3CN) δ 9.10 (d, *J* = 4.7 Hz, 1H, Ar-H), 8.15 (s, 1H, H5-triaz.), 8.09 (td, *J* = 7.7, 1.5 Hz, 1H, Ar-H), 7.76 (d, *J* = 7.7 Hz, 1H, Ar-H), 7.65–7.50 (m, 1H, Ar-H), 6.13 (d, *J* = 15.8 Hz, 1H, CH_2), 5.64 (d, *J* = 15.8 Hz, 1H, CH_2), 4.73 (s, 2H, Fc-H), 4.37 (s, 2H, Fc-H), 4.11 (s, 5H, Fc-H). ^{13}C NMR (151 MHz, DMSO) δ 196.36 (Re-CO), 195.44 (Re-CO), 190.39 (Re-CO), 156.96, 152.52, 147.64, 140.81, 126.93, 126.42, 125.13, 73.51, 69.45, 68.99, 68.96, 67.22, 67.07, 55.02. IR (ATR)/cm^{-1}: 3114 (sp^2 C-H stretch), 3004 (sp^3 C-H stretch), 2024 (M-C≡O sym. stretch), 1931 (M-C≡O asym. stretch), 1904 (M-C≡O asym. stretch), 1581 (sp^2 C=N stretch), 1433 (sp^2 C=C Ar stretch), 1305, 1105, 1076, 1037, 1000, 880, 819, 765, 737, 711. Calc. for $C_{21}H_{16}ClFeN_4O_3Re$: C, 38.81; H, 2.48; N, 8.62, exp. C, 38.99; H, 2.56; N, 8.51.

Complex $4a_{Re}$. Ligand **4a** (150 mg, 0.34 mmol, 1 equiv.), $Re(CO)_5Cl$ (122 mg, 0.34 mmol, 1 equiv.) and chloroform (20 ml) were used for the synthesis. Mobile phase for column chromatography was dichloromethane : methanol = 50 : 1. Yield: **$4a_{Re}$** (0.26 mmol, 76 %), yellow crystals (m. p. = 139–140 °C). Platelet yellow crystals of **$4a_{Re}$** suitable for crystal structure determination were obtained by slow evaporation from a dichloromethane : methanol solution. ^{1}H NMR (300 MHz, DMSO) δ 8.66 (d, *J* = 4.9 Hz, 2H, Ar-H), 8.34 (s, 1H, H5-triaz.), 8.17 (t, *J* = 7.4 Hz, 2H, Ar-H), 7.84 (d, *J* = 8.4 Hz, 2H, Ar-H), 7.41 (t, *J* = 6.5 Hz, 2H, Ar-H), 5.54 (s, 2H, CH_2), 4.87 (s, 2H, Fc-H), 4.32 (s, 2H, Fc-H), 4.04 (s, 5H, Fc-H). ^{13}C NMR (151 MHz, DMSO) δ 196.71 (Re-CO), 192.53 (Re-CO), 155.73, 153.29, 141.76, 141.13, 124.57, 121.45, 117.44, 92.89, 69.79, 66.73, 61.90, 45.76. IR (ATR)/cm^{-1}: 3051 (sp^2 C-H stretch), 2957 (sp^3 C-H stretch), 2917 (sp^3 C-H stretch), 2864 (sp^3 C-H stretch), 2013 (M-C≡O sym. stretch), 1919 (M-C≡O asym. stretch), 1855 (M-C≡O asym. stretch), 1566 (sp^2 C=N stretch), 1461 (sp^2 C=C Ar stretch), 1436 (sp^2 C=C Ar stretch), 1363, 1216, 1040, 996, 867, 787. Calc. for $C_{26}H_{20}ClFeN_6O_3Re$: C, 42.09; H, 2.72; N, 11.33, exp. C, 42.23; H, 2.83; N, 11.45.

Complex $4b_{Re}$. Ligand **4b** (140 mg, 0.31 mmol, 1 equiv.), $Re(CO)_5Cl$ (112 mg, 0.31 mmol, 1 equiv.) and chloroform (20 ml) were used for the synthesis. Mobile phase for column chromatography was dichloromethane : methanol = 50 : 1. Yield: **$4b_{Re}$** (0.25 mmol, 81 %), yellow crystals (m. p. = 225–227 °C). ^{1}H NMR (600 MHz, DMSO) δ 8.62 (d, *J* = 4.9 Hz, 2H, Ar-H), 8.11 (t, *J* = 7.3 Hz, 2H, Ar-H), 7.92 (s, 1H, H5-triaz.), 7.81 (d, *J* = 8.4 Hz, 2H, Ar-H), 7.37 (t, *J* = 6.4 Hz, 2H, Ar-H), 5.48 (s, 2H, CH_2), 5.23 (s, 2H, CH_2), 4.12 (d, *J* = 2.3 Hz, 4H, Fc-H), 3.99 (s, 5H, Fc-H). ^{13}C NMR (151 MHz, DMSO) δ 196.85 (Re-CO), 192.40 (Re-CO), 155.73, 153.19, 141.01, 140.84, 124.58, 121.43, 117.36, 82.54, 68.42, 68.07, 68.01, 48.76, 45.84. IR (ATR)/cm^{-1}: 3091 (sp^2 C-H stretch), 2958 (sp^3 C-H stretch), 2919 (sp^3 C-H stretch), 2012 (M-C≡O sym. stretch), 1901 (M-C≡O asym. stretch), 1851 (M-C≡O asym. stretch), 1736 (sp^2 C=N stretch), 1585 (sp^2 C=C Ar stretch), 1457 (sp^2 C=C Ar stretch), 1432, 1371, 1336, 1216, 1138, 1124, 1105, 1047, 999, 903, 872, 812, 789, 758. Calc. for $C_{27}H_{22}ClFeN_6O_3Re$: C, 42.90; H, 2.93; N, 11.12, exp. C, 43.04; H, 2.98; N, 11.21.

Complex $6a_{Re}$. Ligand **6a** (52 mg, 0.10 mmol, 1 equiv.), $Re(CO)_5Cl$ (36 mg, 0.10 mmol, 1 equiv.) and chloroform (20 ml) were used for the synthesis. Mobile phase for column chromatography was dichloromethane : methanol = 30 : 1. Yield: **$6a_{Re}$** (0.07 mmol, 70 %), orange powder (m. p. = 222–224 °C). ^{1}H NMR (600 MHz, DMSO) δ 9.01 (dd, *J* = 5.6, 1.2 Hz, 1H, Ar-H), 8.76 (d, *J* = 1.9 Hz, 1H, 5H-triaz.), 8.22 (ddd, *J* = 7.7, 4.5, 1.8 Hz, 2H, Ar-H), 7.90–7.85 (m, 2H, Ar-H), 7.79 (td, *J* = 7.7, 1.3 Hz, 1H, Ar-H), 7.70 (ddd, *J* = 7.4, 5.7, 1.4 Hz, 1H, Ar-H), 7.51 (d, *J* = 7.5 Hz, 1H, Ar-H), 7.44 (d, *J* = 2.4 Hz, 1H, Ar-H), 6.96 (dt, *J* = 9.0, 2.4 Hz, 1H, Ar-H), 6.86 (d, *J* = 8.9 Hz, 1H, Ar-H), 6.81 (d, *J* = 9.8 Hz, 1H, Ar-H), 6.43 (dd, *J* = 15.9, 2.1 Hz, 1H, CH_2), 6.40 (dd, *J* = 9.8, 1.9 Hz, 1H), 6.25 (d, *J* = 1.9 Hz, 1H), 5.70 (d, *J* = 15.8 Hz, 1H, CH_2), 5.45 (s, 2H, CH_2), 3.58 (d, *J* = 0.5 Hz, 3H, OCH_3). ^{13}C NMR (151 MHz, DMSO) δ 196.19 (Re-CO), 195.27 (Re-CO), 190.10 (Re-CO), 183.81, 165.15, 162.15, 158.31, 156.98, 153.41, 152.31, 149.94, 143.88, 140.85, 133.79, 133.19. IR (KBr)/cm^{-1}: 2951 (sp^3 C-H stretch), 2922 (sp^3 C-H stretch), 2851, 2027 (M-C≡O sym. stretch), 1926 (M-C≡O asym. stretch), 1900 (M-C≡O asym. stretch), 1723 (ester C=O stretch), 1640 (sp^2 C=N stretch), 1600 (sp^2 C=C Ar stretch), 1512 (sp^2 C=C Ar stretch), 1480, 1457, 1435, 1384, 1284 (C-O stretch), 1209, 1129, 1109, 1081, 1010, 962, 934, 918, 853, 767, 703. Calc. for $C_{33}H_{22}ClN_4O_8Re$: C, 48.09; H, 2.69; N, 6.80, exp. C, 48.26; H, 2.82; N, 6.79.

Complex 9_{Re}. Ligand **9** (31 mg, 0.08 mmol, 1 equiv.), $Re(CO)_5Cl$ (30 mg, 0.08 mmol, 1 equiv.) and chloroform (8 ml) were used for the synthesis. Mobile phase for column chromatography was dichloromethane : methanol = 50 : 1. Yield: **9_{Re}** (0.07 mmol, 91 %), orange powder (m. p. > 250 °C). ^{1}H NMR (600 MHz, DMSO) δ 10.00 (s, 1H, H-triaz.), 9.27–9.07 (m, 2H), 9.02–8.83 (m, 1H), 8.56 (dd, *J* = 4.9, 4.0 Hz, 1H), 8.40 (td, *J* = 7.8, 1.5 Hz, 1H), 8.26–8.04 (m, 2H), 7.86–7.69 (m, 4H), 7.56 (d, *J* = 7.7 Hz, 1H) ppm. ^{13}C NMR (151 MHz, DMSO) δ 197.40 (Re-CO), 196.34 (Re-CO), 189.24 (Re-CO), 153.32, 149.45, 147.95, 144.34, 143.20, 140.84, 139.73, 136.01, 135.18, 130.60, 129.27, 127.20, 126.15, 126.00, 125.82, 124.96, 123.64, 120.87, 117.71, 116.82, 115.35, 111.75, 102.07 ppm. IR (KBr)/cm^{-1}: 3444, 3066 , 3047 (sp^2 C-H stretch), 2958 (sp^3 C-H stretch), 2923 (sp^3 C-H stretch), 2851 (sp^3 C-H stretch), 2377, 2353 (C≡N), 2311, 2239, 2031 (M-C≡O sym. stretch), 1922 (M-C≡O asym. stretch), 1732, 1619 (sp^2 C=N stretch), 1607 (sp^2 C=C Ar stretch), 1470, 1434, 1384, 1288, 1273, 1257, 1184, 1161, 1126, 1101, 1043, 977, 876, 841, 781, 755, 643. Calc. for $C_{26}H_{15}ClN_7O_3Re$: C, 44.93; H, 2.18; N, 14.11, exp. C, 44.99; H, 2.11; N, 14.08.

General procedure for the counterion exchange

To the solution of the complex (1 equiv.) in acetonitrile was added $AgCF_3SO_3$ (1 equiv.) and the reaction mixture was stirred in dark at the reflux temperature for 14 h. After completion of the reaction the solvent was evaporated under reduced pressure. The product was isolated by column chromatography with dichloromethane : methanol = 20 : 1 mixture as a mobile phase.

Complex $4a_{Re}$·OTf. Complex **$4a_{Re}$** (34 mg, 0.046 mmol, 1 equiv.), $AgCF_3SO_3$ (12 mg, 0.046 mmol, 1 equiv.) and acetonitrile (5 ml) were used for the synthesis. Yield: **$4a_{Re}$·OTf** (0.033 mmol, 72 %), orange powder (m. p. = 139–140 °C). ^{1}H NMR (300 MHz, $CDCl_3$) δ 8.90 (d, *J* = 5.5 Hz, 2H, Ar-H), 8.30 (s, 1H, H5-triaz), 8.23–8.00 (m, 4H, Ar-H), 7.42 (t, *J* = 6.4 Hz, 2H, Ar-H), 5.43 (s, 2H, CH_2), 4.86 (d, *J* = 1.7 Hz, 2H, Fc-H), 4.31 (d, *J* = 1.7 Hz, 2H, Fc-H), 4.25 (s, 5H, Fc-H). ^{13}C NMR (151 MHz, $CDCl_3$) δ 194.20, 193.94, 157.01, 153.93, 148.98, 143.61, 126.13, 124.70, 124.65, 120.87 (q, *J* = 320.5 Hz, $CF_3SO_3^-$), 70.65, 67.57, 63.06. IR (KBr)/cm^{-1}: 3445, 3113 (sp^2 C-H stretch), 2958 (sp^3 C-H stretch), 2925 (sp^3 C-H stretch), 2853 (sp^3 C-H stretch), 2034 (M-C≡O sym. stretch), 1912 (M-C≡O asym. stretch), 1709 (sp^2 C=N stretch), 1670 (sp^2 C=N stretch), 1605 (sp^2 C=C Ar stretch), 1472 (sp^2 C=C Ar stretch), 1411, 1385, 1263, 1224, 1157, 1106, 1091, 1071, 1030, 879, 811, 866, 638, 534, 517, 485. Calc. for $C_{27}H_{20}F_3FeN_6O_6ReS$: C. 37.90; H. 2.36; N. 9.82, exp. C. 38.03, H. 2.52, N. 9.71.

Complex $4b_{Re}$·OTf. Complex **$4b_{Re}$** (31 mg, 0.041 mmol, 1 equiv.), $AgCF_3SO_3$ (10.5 mg, 0.041 mmol, 1 equiv.) and acetonitrile (5 ml) were used for the synthesis. Yield: **$4b_{Re}$·OTf** (0.017 mmol, 41 %), orange powder (m. p. = 189–190 °C). Rod-like orange crystals of

$4b_{Re}$·OTf suitable for crystal structure determination were obtained by slow evaporation from a dichloromethane : methanol solution. ^{1}H NMR (600 MHz, $CDCl_3$) δ 8.84 (dd, *J* = 5.6, 1.2 Hz, 2H, Ar-H), 8.13–8.07 (m, 2H, Ar-H), 8.06 (d, *J* = 7.8 Hz, 2H, Ar-H), 7.89 (s, 1H, H5-triaz.), 7.39–7.33 (m, 2H, Ar-H), 5.28 (s, 2H, CH_2), 5.28 (s, 2H, CH_2), 4.36–4.32 (m, 2H, Fc-H), 4.22–4.19 (m, 2H, Fc-H), 4.17 (s, 5H, Fc-H). ^{13}C NMR (151 MHz, $CDCl_3$) δ 194.16 (Re-CO), 193.95 (Re-CO), 156.98, 153.84, 148.87, 143.52, 126.11, 124.55, 120.86 (q, *J* = 320.5 Hz, $CF_3SO_3^-$), 123.85, 78.94, 69.58, 69.38, 68.98, 52.58, 51.87. IR (KBr)/cm^{-1}: 2957 (sp^3 C-H stretch), 2925 (sp^3 C-H stretch), 2853 (sp^3 C-H stretch), 2034 (M-C≡O sym. stretch), 1913 (M-C≡O asym. stretch), 1637 (sp^2 C=N stretch), 1605 (sp^2 C=N stretch), 1472 (sp^2 C=C Ar stretch), 1447 (sp^2 C=C Ar stretch), 1384, 1368, 1262, 1224, 1158, 1030, 813, 766, 638, 481. Calc. for $C_{28}H_{22}F_3FeN_6O_6ReS$: C. 38.67, H. 2.55, N. 9.66, exp. C. 38.81, H. 2.71, N. 9.79.

X-Ray Crystallography

The X-ray intensity data were collected on Oxford diffraction (Xcalibur) or XtaLAB Synergy (Dualflex) CCD diffractometers using monochromatic Cu-Kα (*λ* = 1.54184 Å) radiation. Basic experimental data are given in Table S1. The data were processed with CrysalisPro program,[83] used for unit cell determination and data reduction. Structures were solved by direct methods using SHELXT program[84] and refined against F^2 on all data by a full-matrix least squares procedure with SHELXL program.[85] All non-hydrogen atoms were refined in an anisotropic model of atomic displacement parameters.

The structures of two ligand compounds **2b** and **3** were solved and refined without any difficulties and they are represented in usual structural model in which hydrogen atoms are included at geometrically calculated positions. Due to observation of two distinctive peaks in difference electron density map corresponding to two opposite positions of *ortho*-hydrogen atom from pyridine unit in **3**, occupancies of both orientations of pyridine unit were refined and additional "rigid body" restraints were added (RIGU restraints). The refined occupancy for the "*cis*" orientation is 0.64(3) and for the "*trans*" orientation is 0.36(3). The orientation in which torsion angle N1-C6-C7-N12 is ≈ 60° or ≈ –120° are taken as "*cis*" or "*trans*" orientations, respectively (Figure S3). Regarding structures with Re atoms (**$2a_{Re}$**, **3_{Re}**, **$4a_{Re}$** and **$4b_{Re}$·OTf**) the residual electron density around Re atoms in all structures showed significant deviations. The lowest quality data were for **$4a_{Re}$** [R_{int} = 11.60 %, the fraction of unique reflections measured up to *Θ* of 67.68° is 0.93, with significant number of missing reflections (336)] which leaded to structure having high *R* values (Table S1), although the structure was undoubtedly solved by SHELXT and least square cycles of SXELXL refinement showed convergence of all parameters (Δ_{max}/su ≈ 0). In order to prevent unphysical behaviour of the anisotropic displacement parameters for non-hydrogen atoms, the "rigid body" restraints were added to all atoms in the last refinement cycles. Data for structure **3_{Re}** were of better quality (R_{int} = 7.55 %, the fraction of unique reflections measured up to *Θ* of 67.68° is 0.985). Despite of this better data set quality, the four residual peaks of difference electron density in the vicinity of Re atoms were unusually high (above 5 el/Å^3) (two Re atoms from two molecules in the asymmetric unit). Because all atoms bonded to Re should be ≈ 2 Å distant and peaks were located at distance close to 1 Å from Re atoms, it is assumed that additional peaks come from other, less occupied positions of the whole molecules. Because the Re atom is the heaviest, the less occupied positions of other atoms are probably immersed in the noise of electron density. Therefore, in the last refinement cycles the highest peaks around Re atoms were treated as lower occupied positions of nearby Re atoms with restraint that sum of occupations for each position in one Re group is 1. Such treatment was already encountered in the structure of Re(5-H_2NCO-phen)(CO)$_3$Cl[86] and it was treated in the same way. Similar to the results of Kemmerdy et all,[86] refined occupancies for the central, most populated positions of Re1 and Re2 atoms in each Re group were above 0.93, while additional nearby peaks represent disordered Re atoms with occupancies below 0.04. Additionally, due to large displacement parameters of carbon atom from ferrocene units, the rigid body restraint was used. Although the most significant peaks of difference electron density for **$2a_{Re}$** were also in the vicinity of Re atoms, they were not as much high as for **3_{Re}**, therefore additional modelling of the disorder of Re atoms were not performed for **$2a_{Re}$**. The only observation is that displacement parameters on atoms of the free cyclopentadienyl ring of ferrocene unit were significantly larger than displacement parameters on other atoms, so rigid body restraints were used for atoms of the ferrocene unit. Only in the structure of **$4b_{Re}$·OTf**, (the only structure without Cl^- anion coordinating the Re atom) the highest peak in the difference electron density is in the vicinity of the S atom from the triflate anion. This anion shows enlarged displacement parameters and one additional, disordered molecule of chloroform is recognized in the structure. The CCDC 2254508-2254513 contain the supplementary crystallographic data for this paper. These data can be obtained free of charge from The Cambridge Crystallographic Data Centre via www.ccdc.cam.ac.uk/data_request/cif.

Interactions with biomolecules

Aqueous buffer solution (pH = 7.0, *I* = 0.05 M, sodium cacodylate buffer) was used for all the measurements. UV-Vis spectra were recorded on a Varian Cary 100 Bio spectrometer, fluorescence spectra were recorded on a Varian Cary Eclipse fluorimeter and CD spectra were recorded on a JASCO J815 spectropolarimeter. Fluorescence decay measurements were performed on Edinburgh Instruments FS5 Spectrofluorometer by time-correlated single-photon counting (TC-SPC), and absolute quantum yields were determined using the Integrating sphere SC-30 on FS5 Spectrofluorometer. All measurements were taken at 25.0 °C using appropriate quartz cuvettes with a path length of 1 cm.

Polynucleotides were purchased as noted: calf thymus (ct)–DNA (Sigma Aldrich), poly A–poly U (Sigma Aldrich) and dissolved in sodium cacodylate buffer. ct-DNA was additionally sonicated and filtered through a 0.45 mm filter to obtain mostly short rod-like

B-helical DNA fragments.[87] Polynucleotide concentration was determined as the concentration of phosphates (corresponds to *c*(nucleobase), λ_{max} = 260 nm) spectroscopically.[76] Human serum albumin (HSA, Sigma Aldrich) was dissolved in milliQ water at a concentration of $c = 1 \times 10^{-3}$ M.

Fluorimetric titrations were performed by adding DNA, RNA or protein stock solution aliquots into buffered solutions of fluorophores and collecting emission spectra. Titration data were processed by means of Scatchard equation (for DNA, RNA),[73] yielding binding constants; whereas titration with HSA gave the best fit for the 1 : 1 stoichiometry dye : HSA.

Thermal denaturation experiments were done in aqueous buffer by measuring the absorption change of polynucleotides and their complexes at 260 nm as a function of temperature. T_m values were determined from the maximum of the first derivative and represent the midpoints of the transition curves. ΔT_m values were obtained by subtraction of the T_m of free nucleic acid from the T_m of the complex of nucleic acid and compound. T_m values reported here are averages of at least two measurements and the error in ΔT_m is ± 0.5 °C.

Circular dichroism (CD) studies were conducted in aqueous buffer with a scanning speed of 200 nm/min and averaging 3 accumulations. The titrations were performed by addition of compound solutions into polynucleotide solution ($c = 2 \times 10^{-5}$ M) and background (buffer) was subtracted from each measurement.

Cell Culture

The CT-26 cell line was cultured in DMEM medium, the HT-29 cell line in McCoy's 5A (modified) medium and the RPE-1 cell line in DMEM-F12 medium. All cell line media were supplemented with 10% fetal calf serum (Gibco) and 1% Penicillin-Streptomycin antibiotic (Gibco). Cell lines were maintained in a humidified atmosphere at 37 °C with 5% CO_2.

Cytotoxicity Assay Using a 2D Cellular Model

The cytotoxicity of the tested complexes was assessed by a fluorometric cell viability assay using Resazurin (Acros Organics). Cells were seeded in triplicates in 96-well plates (100 µl/well). Cells were seeded at a 4×10^3 cells/ well for CT26, 5×10^3 cells/ well for HT29 and 10×10^3 cells/ well for RPE-1. After 24 h, cells were treated with increasing concentrations of the Re complexes and CDDP control. Dilutions for complexes were prepared as follows: 10 mM stock in DMSO was diluted to 100–0.01 µM with media. After 48 h of incubation, the medium was removed, and 100 µL of complete medium containing resazurin (0.2 mg/mL final concentration) was added. After 4 h of incubation at 37 °C, the fluorescence signal of the resorufin product was read (λ_{ex} 540 nm, λ_{em} 590 nm) in an Infinite 200 PRO Microplate Reader from TECAN. IC_{50} values were then calculated using GraphPad Prism software.

Cellular localization

CT26 cells (5×10^4 cells) were seeded in 35 mm culture dishes for 24 h. Cell medium was then replaced by fresh medium containing 7 µM of $\mathbf{9_{Re}}$. After incubation for 3h at 37 °C, cells were washed with PBS. Cells were then labelled with LysoTracker™ Deep Red (Thermofisher, 500 nM) at 37 °C for 10 min. Live cells were imaged in a confocal laser scanning microscope (Leica SP8) equipped with a x63/1.40 plan apochromatic objective. The LysoTracker™ Deep Red was excited at 638 nm and its emission collected between 650 and 750 nm (displayed in cyan). Complex $\mathbf{9_{Re}}$ was excited at 405 nm and its fluorescence collected between 415 and 550 nm (displayed in magenta). The negative control is shown in Figures S101 and S102 and the confocal imaging of the complex in Figures S103 and S104.

Conflicts of interest

There are no conflicts to declare.

Acknowledgements

This work was supported by CAT Pharma (KK.01.1.1.04.0013) project, co-financed by the Croatian Government and the European Union through the European Regional Development Fund–the Competitiveness and Cohesion Operational Programme. Support by a Croatian–French bilateral project (MSE–Cogito) is gratefully acknowledged. L. G. acknowledges the ENS-PSL for her PhD fellowship. This work was also financially supported by an ERC Consolidator Grant PhotoMedMet to G.G. (GA 681679), has received support under the program "Investissements d'Avenir" launched by the French Government and implemented by the ANR with the reference ANR-10-IDEX-0001-02 PSL (G.G.). I.P. and I.C. acknowledge financial support for DNA, RNA, protein studies by Croatian Science Foundation project IP-2018-01-5475.

Notes and references

1 S. A. Aldossary, *Biomed. Pharmacol. J.*, 2019, **12**, 07–15.

2 B. Köberle and S. Schoch, *Cancers*, 2021, **13**, 2073.
3 J. T. Hartmann and H.-P. P. Lipp, *Expert Opin. Pharmacother.*, 2003, **4**, 889–901.
4 Y. Jung and S. J. Lippard, *Chem. Rev.*, 2007, **107**, 1387–1407.
5 M. A. Jakupec, M. Galanski and B. K. Keppler, *Rev. Physiol. Biochem. Pharmacol.*, 2003, **146**, 1–54.
6 P. V Simpson, N. M. Desai, I. Casari, M. Massi and M. Falasca, *Future Med. Chem.*, 2019, **11**, 119–135.
7 E. B. Bauer, A. A. Haase, R. M. Reich, D. C. Crans and F. E. Kühn, *Coord. Chem. Rev.*, 2019, **393**, 79–117.
8 G. Gasser, I. Ott and N. Metzler-Nolte, *J. Med. Chem.*, 2011, **54**, 3–25.
9 U. Ndagi, N. Mhlongo and M. Soliman, *Drug Des. Devel. Ther.*, 2017, **11**, 599–616.
10 E. Boros, P. J. Dyson and G. Gasser, *Chem*, 2020, **6**, 41–60.
11 P. Köpf-Maier, H. Köpf and E. W. Neuse, *Angew. Chemie Int. Ed.*, 1984, **23**, 456–457.
12 D. R. van Staveren and N. Metzler-Nolte, *Chem. Rev.*, 2004, **104**, 5931–5986.
13 A. Singh, G. Fong, J. Liu, Y.-H. Wu, K. Chang, W. Park, J. Kim, C. Tam, L. W. Cheng, K. M. Land and V. Kumar, *ACS Omega*, 2018, **3**, 5808–5813.
14 R. Wang, H. Chen, W. Yan, M. Zheng, T. Zhang and Y. Zhang, *Eur. J. Med. Chem.*, 2020, **190**, 112109.
15 M. Patra and G. Gasser, *Nat. Rev. Chem.*, 2017, **1**, 0066.
16 B. Sharma and V. Kumar, *J. Med. Chem.*, 2021, **64**, 16865–16921.
17 E. Hillard, A. Vessières, L. Thouin, G. Jaouen and C. Amatore, *Angew. Chem. Int. Ed.*, 2006, **45**, 285–290.
18 G. Jaouen, A. Vessières and S. Top, *Chem. Soc. Rev.*, 2015, **44**, 8802–8817.
19 C. Biot, G. Glorian, L. A. Maciejewski, J. S. Brocard, O. Domarle, G. Blampain, P. Millet, A. J. Georges, H. Abessolo, D. Dive and J. Lebibi, *J. Med. Chem.*, 1997, **40**, 3715–3718.
20 W. A. Wani, E. Jameel, U. Baig, S. Mumtazuddin and L. T. Hun, *Eur. J. Med. Chem.*, 2015, **101**, 534–551.
21 A. Kondratskyi, K. Kondratska, F. Vanden Abeele, D. Gordienko, C. Dubois, R. A. Toillon, C. Slomianny, S. Lemière, P. Delcourt, E. Dewailly, R. Skryma, C. Biot and N. Prevarskaya, *Sci. Rep.*, 2017, **7**, 1–15.
22 B. Weber, A. Serafin, J. Michie, C. Van Rensburg, J. C. Swarts and L. Bohm, *Anticancer Res.*, 2004, **24**, 763–770.
23 J. Oyarzo, A. Acuña, H. Klahn, R. Arancibia, C. P. Silva, R. Bosque, C. López, M. Font-Bardía, C. Calvis and R. Messeguer, *Dalton Trans.*, 2018, **47**, 1635–1649.
24 Y. Kuninobu and K. Takai, *Chem. Rev.*, 2010, **111**, 1938–1953.
25 L. Suntrup, F. Stein, J. Klein, A. Wilting, F. G. L. Parlane, C. M. Brown, J. Fiedler, C. P. Berlinguette, I. Siewert and B. Sarkar, *Inorg. Chem.*, 2020, **59**, 4215–4227.
26 H. S. Liew, C.-W. Mai, M. Zulkefeli, T. Madheswaran, L. V. Kiew, N. Delsuc and M. L. Low, *Molecules*, 2020, **25**, 4176.
27 S. C. Marker, S. N. MacMillan, W. R. Zipfel, Z. Li, P. C. Ford and J. J. Wilson, *Inorg. Chem.*, 2018, **57**, 1311–1331.
28 J. Berrones Reyes, M. K. Kuimova and R. Vilar, *Curr. Opin. Chem. Biol.*, 2021, **61**, 179–190.
29 F. L. Thorp-Greenwood, M. P. Coogan, L. Mishra, N. Kumari, G. Rai and S. Saripella, *New J. Chem.*, 2012, **36**, 64–72.
30 T. A. Gillam, C. Caporale, R. D. Brooks, C. A. Bader, A. Sorvina, M. V. Werrett, P. J. Wright, J. L. Morrison, M. Massi, D. A. Brooks, S. Zacchini, S. M. Hickey, S. Stagni and S. E. Plush, *Inorg. Chem.*, 2021, **60**, 10173–10185.
31 A. Leonidova and G. Gasser, *ACS Chem. Biol.*, 2014, **9**, 2180–2193.
32 P. Collery, D. Desmaele and V. Vijaykumar, *Curr. Pharm. Des.*, 2019, **25**, 3306–3322.
33 C. C. Konkankit, S. C. Marker, K. M. Knopf and J. J. Wilson, *Dalton Trans.*, 2018, **47**, 9934–9974.
34 V. L. Gantsho, M. Dotou, M. Jakubaszek, B. Goud, G. Gasser, H. G. Visser and M. Schutte-Smith, *Dalton Trans.*, 2020, **49**, 35–46.
35 J. Delasoie, A. Pavic, N. Voutier, S. Vojnovic, A. Crochet, J. Nikodinovic-Runic and F. Zobi, *ChemRxiv*, , DOI:10.26434/chemrxiv.12012840.
36 K. M. Knopf, B. L. Murphy, S. N. Macmillan, J. M. Baskin, M. P. Barr, E. Boros and J. J. Wilson, *J. Am. Chem. Soc.*, 2017, **139**, 14302–14314.
37 H. Struthers, T. L. Mindt and R. Schibli, *Dalton Trans.*, 2009, **39**, 675–696.
38 D. Schweinfurth, L. Hettmanczyk, L. Suntrup and B. Sarkar, *Zeitschrift für Anorg. und Allg. Chemie*, 2017, **643**, 554–584.
39 N. Pantalon Juraj, M. Krklec, T. Novosel, B. Perić, R. Vianello, S. Raić-Malić and S. I. Kirin, *Dalton Trans.*, 2020, **49**, 9002–9015.
40 L. Suntrup, S. Klenk, J. Klein, S. Sobottka and B. Sarkar, *Inorg. Chem.*, 2017, **56**, 5771–5783.
41 S. Clède, F. Lambert, R. Saint-Fort, M.-A. Plamont, H. Bertrand, A. Vessières and C. Policar, *Chem. Eur. J.*, 2014, **20**, 8714–8722.
42 J. Li, R. Abel, K. Zhu, Y. Cao, S. Zhao and R. A. Friesner, *Proteins Struct. Funct. Bioinforma.*, 2011, **79**, 2794-2812.
43 S. B. Wagh, V. A. Maslivetc, J. J. La Clair and A. Kornienko, *ChemBioChem*, 2021, **22**, 3109–3139.
44 L. Wei, J. W. Babich, W. Ouellette and J. Zubieta, *Inorg. Chem.*, 2006, **45**, 3057–3066.
45 N. Viola-Villegas, A. E. Rabideau, M. Bartholoma, J. Zubieta and R. P. Doyle, *J. Med. Chem.*, 2009, **52**, 5253–5261.
46 M. W. Louie, T. T. H. Fong and K. K. W. Lo, *Inorg. Chem.*, 2011, **50**, 9465–9471.
47 L. C. C. Lee, K. K. Leung and K. K. W. Lo, *Dalton Trans.*, 2017, **46**, 16357–16380.
48 M. Howe-Grant and S. J. Lippard, *Biochemistry*, 1979, **18**, 5762–5769.
49 B. Jadoo, I. N. Booysen, M. P. Akerman, L. Rhyman and P. Ramasami, *Polyhedron*, 2018, **144**, 107–118.
50 Y. Sha, X. Chen, B. Niu and Q. Chen, *Chem. Biodivers.*, 2017, **14**, e1700133.

51 M. Ashfaq, T. Najam, S. S. A. Shah, M. M. Ahmad, S. Shaheen, R. Tabassum and G. Rivera, *Curr. Med. Chem.*, 2014, **21**, 3081–3094.
52 C. Metcalfe and J. A. Thomas, *Chem. Soc. Rev.*, 2003, **32**, 215.
53 N. Raman and S. Sobha, *Spectrochim. Acta Part A Mol. Biomol. Spectrosc.*, 2012, **85**, 223–234.
54 M. Kaplanis, G. Stamatakis, V. D. Papakonstantinou, M. Paravatou-Petsotas, C. A. Demopoulos and C. A. Mitsopoulou, *J. Inorg. Biochem.*, 2014, **135**, 1–9.
55 A. Meščić Macan, N. Perin, S. Jakopec, M. Mioč, M. R. Stojković, M. Kralj, M. Hranjec and S. Raić-Malić, *Eur. J. Med. Chem.*, 2020, **185**, 111845.
56 S. Jakopec, N. Pantalon Juraj, A. Brozovic, D. Jadreško, B. Perić, S. I. Kirin and S. Raić-Malić, *Appl. Organomet. Chem.*, 2022, **36**, e6575.
57 M. Šranková, A. Dvořák, M. Martínek, P. Šebej, P. Klán, L. Vítek and L. Muchová, *Int. J. Mol. Sci.*, 2022, **23**, 1504.
58 M. Rajasekar, *J. Mol. Struct.*, 2021, **1224**, 129085.
59 T. Romero, R. A. Orenes, A. Espinosa, A. Tárraga and P. Molina, *Inorg. Chem.*, 2011, **50**, 8214–8224.
60 J. D. Crowley, P. H. Bandeen and L. R. Hanton, *Polyhedron*, 2010, **29**, 70–83.
61 B. M. Upton, R. M. Gipson, S. Duhović, B. R. Lydon, N. M. Matsumoto, H. D. Maynard and P. L. Diaconescu, *Inorg. Chem. Front.*, 2014, **1**, 271.
62 G.-C. Kuang, H. A. Michaels, J. T. Simmons, R. J. Clark and L. Zhu, *J. Org. Chem.*, 2010, **75**, 6540–6548.
63 M. Obata, A. Kitamura, A. Mori, C. Kameyama, J. A. Czaplewska, R. Tanaka, I. Kinoshita, T. Kusumoto, H. Hashimoto, M. Harada, Y. Mikata, T. Funabiki and S. Yano, *Dalton Trans.*, 2008, 3292.
64 H. C. Bertrand, S. Clède, R. Guillot, F. Lambert and C. Policar, *Inorg. Chem.*, 2014, **53**, 6204–6223.
65 S. Fery-Forgues and B. Delavaux-Nicot, *J. Photochem. Photobiol. A Chem.*, 2000, **132**, 137–159.
66 Y. Xiang, B. He, X. Li and Q. Zhu, *RSC Adv.*, 2013, **3**, 4876–4879.
67 J. R. Farrell, G. J. Kerins, K. L. Niederhoffer, L. A. Crandall and C. Ziegler, *J. Organomet. Chem.*, 2016, **813**, 41–45.
68 X. Li, H. Zhang, Y. Xie, Y. Hu, H. Sun and Q. Zhu, *Org. Biomol. Chem.*, 2014, **12**, 2033.
69 G. Jaouen, *Bioorganometallics: biomolecules, labeling, medicine*, John Wiley & Sons, 2006.
70 A. Caballero, A. Espinosa, A. Tárraga and P. Molina, *J. Org. Chem.*, 2008, **73**, 5489–5497.
71 Y. Yamaguchi, W. Ding, C. T. Sanderson, M. L. Borden, M. J. Morgan and C. Kutal, *Coord. Chem. Rev.*, 2007, **251**, 515–524.
72 X. Lee, Philbert ; Wu, *Curr Pharm Des*, 2017, **176**, 139–148.
73 G. D. Scatchard, *Ann. N. Y. Acad. Sci.*, 1949, **51**, 660–672.
74 M. Eriksson and B. Nordén, *Methods Enzymol.*, 2001, **340**, 68–98.
75 T. Šmidlehner, I. Piantanida and G. Pescitelli, *Beilstein J. Org. Chem.*, 2018, **14**, 84–105.
76 J. L. Mergny and L. Lacroix, *Oligonucleotides*, 2003, **13**, 515–537.
77 W. D. Wilson, L. Ratmeyer, M. Zhao, L. Strekowski and D. Boykin, *Biochemistry*, 1993, **32**, 4098–4104.
78 W. K. C. Lo, G. S. Huff, J. R. Cubanski, A. D. W. Kennedy, C. J. McAdam, D. A. McMorran, K. C. Gordon and J. D. Crowley, *Inorg. Chem.*, 2015, **54**, 1572–1587.
79 K. Qiu, H. Huang, B. Liu, Y. Liu, Z. Huang, Y. Chen, L. Ji and H. Chao, *ACS Appl. Mater. Interfaces*, 2016, **8**, 12702–12710.
80 K. Qiu, H. Zhu, T. W. Rees, L. Ji, Q. Zhang and H. Chao, *Coord. Chem. Rev.*, 2019, **398**, 113010.
81 Z. Yan, G. Wei, S. Guang, M. Xu, X. Ren, R. Wu, G. Zhao, F. Ke and H. Xu, *Dyes Pigm.*, 2018, **159**, 542–550.
82 T. Y. Kim, A. B. S. Elliott, K. J. Shaffer, C. John McAdam, K. C. Gordon and J. D. Crowley, *Polyhedron*, 2013, **52**, 1391–1398.
83 Rigaku Oxford Diffraction CrysAlisPro, 2018.
84 G. M. Sheldrick, *Acta Crystallogr. Sect. A Found. Adv.*, 2015, **71**, 3–8.
85 G. M. Sheldrick, *Acta Crystallogr. Sect. C Struct. Chem.*, 2015, **71**, 3–8.
86 V. Komreddy, K. Ensz, H. Nguyen, D. P. Rillema and C. E. Moore, *J. Mol. Struct.*, 2021, **1223**, 128739.
87 L. N. Schulte, B. Heinrich, H. Janga, B. T. Schmeck and O. Vázquez, *Angew. Chem. Int. Ed.*, 2018, **57**, 11564–11568.